IRE1/XBP1 signaling promotes skeletal muscle regeneration through a cell non-autonomous mechanism

By

Anirban Roy[1], Meiricris Tomaz da Silva[1], Raksha Bhat[1], Kyle R. Bohnert[2], Takao Iwawaki[3], and Ashok Kumar[1,*]

[1]Department of Pharmacological and Pharmaceutical Sciences, University of Houston College of Pharmacy, Houston, TX 77204, USA

[2]Kinesiology Department, St. Ambrose University, Davenport, IA, USA

[3]Division of Cell Medicine, Department of Life Science, Medical Research Institute, Kanazawa Medical University, Uchinada, Japan

***Corresponding author:**

Ashok Kumar, Ph.D.
Department of Pharmacological and Pharmaceutical Sciences
Health Building 2, Room 5012
College of Pharmacy
University of Houston
4849 Calhoun Road
Houston, TX 77204-1217

Phone: 713-743-3376
Email: akumar43@Central.UH.EDU

Key words: Skeletal muscle regeneration,

Running title: IRE1 regulates regenerative myogenesis

Abstract

Skeletal muscle regeneration is regulated by coordinated activation of multiple signaling pathways activated in both injured myofibers and satellite cells. The unfolded protein response (UPR) is a major mechanism that detects and alleviates protein-folding stresses in ER. However, the role of individual arms of the UPR in skeletal muscle regeneration remain less understood. In the present study, we demonstrate that IRE1α-XBP1 pathway is activated in skeletal muscle of mice upon injury. Myofiber-specific deletion of IRE1 or XBP1 in mice diminishes skeletal muscle regeneration accompanied with reduced number of satellite cells and their fusion to injured myofibers. Ex vivo cultures of myofiber explants demonstrate that ablation of IRE1α reduces the proliferative capacity of myofiber-associated satellite cells. Myofiber-specific deletion of IRE1α dampens Notch signaling and canonical NF-κB pathway in skeletal muscle of mice. Our results also demonstrate that targeted ablation of IRE1α reduces skeletal muscle regeneration in the mdx model of Duchenne muscular dystrophy. Collectively, our results reveal that the IRE1α-mediated signaling promotes muscle regeneration through augmenting the proliferation of satellite cells in a cell non-autonomous manner.

Introduction

Skeletal muscle, the most abundant tissue of the body, has remarkable regenerative capacity mainly due to its resident muscle stem cells, also known as satellite cells. These cells are located beneath the basal lamina of myofiber in a dormant state. Upon muscle injury, satellite cells become activated leading to their asymmetric cell division and differentiation into myoblasts which eventually fuse together or with existing myofibers to accomplish muscle regeneration (Kuang and Rudnicki, 2008; Yin et al., 2013). In many muscle diseases, such as Duchenne muscular dystrophy (DMD) and aged skeletal muscle (sarcopenia), the abundance and regenerative capacity of satellite cells is diminished leading to impairment in muscle regeneration and a net loss of muscle mass (Brack and Munoz-Canoves, 2016; Dumont et al., 2015). It is now increasingly evidenced that muscle regeneration is regulated through orchestrated activation of multiple signaling pathways and factors produced by regenerating myofiber as well as other cell types (Dumont et al., 2015). However, the mechanisms of muscle regeneration are not yet fully understood.

The endoplasmic reticulum (ER) is the major subcellular compartment that is involved in protein folding and secretion. Many secreted proteins are translated from mRNAs localized on the cytosolic side of the ER membrane and enter the ER as nascent chains that are modified and properly folded before exiting the organelle (Harding et al., 1999). An imbalance between the influx of unfolded proteins and the capacity of the organelle to handle them cause stress in the ER that triggers activation of an adaptive signaling network, known as the unfolded protein response (UPR) (Hetz, 2012; Preissler and Ron, 2019; Wang and Kaufman, 2014). The major goal of the UPR is to restore homeostasis or induce apoptosis of permanently damaged cells (Tabas and Ron, 2011). The UPR is initiated by three ER transmembrane sensors: RNA-dependent protein kinase-like ER eukaryotic translation initiation factor 2 alpha kinase (PERK), inositol-requiring enzyme 1 (IRE1), and activating transcription factor 6 (ATF6). PERK directly phosphorylates eukaryotic translation initiation factor 2 α (eIF2α), which leads to the attenuation of translation initiation and limits the protein-folding load on the ER. IRE1α is a serine/threonine kinase and endoribonuclease controlling cell fate under ER stress. Once activated, IRE1α oligomerizes leading to three major downstream outputs: the activation of c-Jun N-terminal kinase (JNK), the splicing of XBP1 mRNA, and the degradation of targeted mRNA and

microRNAs, a process referred to as regulated IRE1-dependent decay (RIDD) (Hollien et al., 2009; Hollien and Weissman, 2006; Maurel et al., 2014; Wang and Kaufman, 2014). Upon stress in ER, ATF6 protein is transported to the Golgi complex where it is cleaved by S1P and S2P to release the N-terminal-domain. The cleaved ATF6 domain translocates to the nucleus, where in association with other factors, it induces gene transcription of target molecules such as GRP78, GRP94 and calnexin (Hetz, 2012; Walter and Ron, 2011; Wang and Kaufman, 2014). Although ER stress is the major stimuli, a few components of the UPR, including IRE1α and XBP1 can also be activated in the absence of ER stress (Abdullah and Ravanan, 2018; Dufey et al., 2020; Martinon et al., 2010).

Accumulating evidence suggests that the UPR plays an important role in the regulation of skeletal muscle mass and regenerative myogenesis (Afroze and Kumar, 2019; Bohnert et al., 2018). ATF6 arm of the UPR is activated during skeletal muscle development where it mediates apoptosis of a subpopulation of myoblasts that may be incompetent of handling cellular stresses (Nakanishi et al., 2005). The role of the UPR in myogenesis is also supported by the findings that pan-inhibition of ER stress attenuates apoptosis and myogenic differentiation (Nakanishi et al., 2005) whereas inducers of ER stress remove vulnerable myoblasts allowing more efficient differentiation into myotubes in cell cultures (Nakanishi et al., 2007). Recent studies have suggested that PERK arm of the UPR is required for maintaining satellite cells in a quiescent state in skeletal muscle of adult mice. Genetic inducible ablation of PERK in satellite cells inhibits skeletal muscle regeneration in adult mice (Xiong et al., 2017; Zismanov et al., 2016). Intriguingly, a very recent study demonstrated that IRE1α promotes skeletal muscle regeneration through RIDD-mediated reduction in myostatin levels (He et al., 2021). However, the role and the mechanisms by which the IRE1α/XBP1 signaling in myofiber regulates skeletal muscle regeneration in adult mice remain poorly understood.

In the present study, using genetic mouse models, we have investigated the role of IRE1 and XBP1 in skeletal muscle regeneration. Our results demonstrate myofiber-specific ablation of IRE1α attenuates skeletal muscle regeneration in adult mice. IRE1α controls muscle regeneration through the activation of XBP1 transcription factor, but not through RIDD mechanism. Genetic ablation of XBP1 also reduces regeneration of injured skeletal muscle. Our results also

demonstrate that IRE1α/XBP1 pathway in myofiber regulates the proliferation of satellite cells in a non-cell-autonomous manner potentially through the activation of Notch signaling. Finally, our experiments demonstrate that genetic ablation of IRE1α exacerbates myopathy and reduces the number of satellite cells in skeletal muscle of dystrophin-deficient mdx (a model of DMD) mice.

Results

Myofiber-specific deletion of IRE1α attenuates skeletal muscle regeneration in adult mice. We first investigated how the phosphorylation of IRE1α and levels of spliced XBP1 (sXBP1) protein are regulated in skeletal muscle after injury. Left side tibialis anterior (TA) muscle of wild-type (WT) mice was injected with 1.2% $BaCl_2$ solution, a widely used myotoxin for experimental muscle injury (Hindi et al., 2017; Xiong et al., 2017), whereas contralateral TA muscle was injected with saline only to serve as control. Results showed that the levels of phosphorylated IRE1α were significantly increased in TA muscle at day 5 post-injury compared to contralateral control muscle. Furthermore, the levels of spliced XBP1 (sXBP1) protein were also found to be considerably increased in injured TA muscle of mice suggesting activation of the IRE1α/XBP1 pathway in injured muscle (**Figure 1A**).

We next sought to investigate the role of IRE1α in skeletal muscle regeneration. Floxed Ire1 (henceforth $Ire1^{fl/fl}$) mice were crossed with muscle creatine kinase (MCK)-Cre to generate $Ire1^{fl/fl}$;MCK-Cre (henceforth $Ire1^{mKO}$) and littermate $Ire1^{fl/fl}$ mice. There was no significant difference in their body weight or muscle weight of $Ire1^{fl/fl}$ and $Ire1^{mKO}$ mice in naïve conditions (data not shown). Western blot analysis confirmed that levels of IRE1α protein were considerably reduced in TA and soleus muscle, but not in liver of $Ire1^{mKO}$ mice (**Figure 1B**). To understand the role of IRE1α signaling in muscle regeneration, TA muscle of 3-month old littermate $Ire1^{fl/fl}$ and $Ire1^{mKO}$ mice was injected with 50 µl of 1.2% $BaCl_2$ solution to induce necrotic muscle injury. Muscle regeneration was evaluated at day 5 and day 14 post-$BaCl_2$ injection by performing Hematoxylin and Eosin (H&E) staining (**Figure 1C**). Results showed that the regeneration of TA muscle was attenuated in $Ire1^{mKO}$ mice compared to $Ire1^{fl/fl}$ mice at day 5 post-injury. There was an apparent decrease in the size of centronucleated myofibers (CNFs) and an increase in the cellular infiltrate in $Ire1^{mKO}$ mice compared to $Ire1^{fl/fl}$ mice (**Figure 1C**). Morphometric analysis H&E-stained TA muscle sections revealed a significant decrease in the average cross-sectional area (CSA) and minimal Feret's diameter of regenerating

myofibers in Ire1^{mKO} mice compared with Ire1$^{fl/fl}$ mice (**Figure 1D-F**). Moreover, the percentage of myofibers containing two or more centrally located nuclei was significantly reduced in injured TA muscle of Ire1^{mko} mice compared with Ire1$^{fl/fl}$ mice (**Figure 1G**). Deficits in muscle regeneration in Ire1^{mKO} mice were also present at day 14 after muscle injury (**Figure 1C, 1F & 1G**).

We also studied TA muscle regeneration in Ire1$^{fl/fl}$ and Ire1^{mKO} mice after performing double injury. At day 21 of first injury, TA muscle of Ire1$^{fl/fl}$ and Ire1^{mKO} mice was injured again by intramuscular injection of 50 μl 1.2% $BaCl_2$ solution. After 5 days, the muscle was isolated and analyzed by performing H&E staining (**Figure 1H**). Results showed that defect in muscle regeneration in Ire1^{mKO} mice was more pronounced after second round of injury. Moreover, Masson's Trichrome staining of TA muscle sections showed considerably increase in deposition of fibrotic tissue at day 5 after second injury (**Figure 1I**).

Ablation of IRE1α reduces the expression of early markers of muscle regeneration in mice. To further understand the role of IRE1α in skeletal muscle regeneration, we studied the expression of early markers of regeneration such embryonic myosin heavy chain (eMyHC) and various myogenic regulatory factors (MRFs). We first analyzed 5d-injured TA muscle of Ire1$^{fl/fl}$ and Ire1^{mko} mice by immunostaining for eMyHC and laminin protein. Nuclei were counterstained with DAPI (4′,6-diamidino-2-phenylindole). Results showed that the proportion of eMyHC^{+} myofibers within laminin staining with higher cross-sectional area (CSA) were reduced in TA muscle of Ire1^{mKO} mice compared to Ire1$^{fl/fl}$ mice (**Figure 2A, 2B**). Moreover, the percentage of eMyHC^{+} myofibers containing 2 or more centrally located nuclei was significantly reduced in regenerating TA muscle of Ire1^{mKO} mice compared with Ire1$^{fl/fl}$ mice (**Figure 2C**). Skeletal muscle regeneration involves a sequential up-regulation of Myf5, MyoD, myogenin, and eMyHC. Our qPCR analysis showed that there was no significant difference in the mRNA levels of eMyHC, Myf5, MyoD, and myogenin in uninjured TA muscle of Ire1$^{fl/fl}$ and Ire1^{mko} mice. However, mRNA levels of Myf5, MyoD, myogenin, and eMyHC were found to be significantly reduced in 5d-injured TA muscle of Ire1^{mko} mice compared to 5d-injured TA muscle of Ire1$^{fl/fl}$ mice (**Figure 2D-2G**). Furthermore, western blot analysis showed that protein levels of MyoD and eMyHC, but not myogenin, were considerably reduced in 5d-injured TA muscle of Ire1^{mko}

mice compared to Ire1$^{fl/fl}$ mice (**Figure 2H**). Collectively, these results suggest that myofiber-specific ablation of Ire1α attenuates regenerative myogenesis in adult mice.

Ablation of IRE1α reduces abundance of satellite cells in regenerating skeletal muscle. Since satellite cells are indispensable for muscle repair (Yin et al., 2013), we next investigated whether myofiber-specific ablation of IRE1α affects the number of satellite cells in injured skeletal muscle. Pax7 is a transcription factor that is expressed in both quiescent and activated satellite cells (Dumont et al., 2015). Indeed, Pax7 has been widely used as a marker to label and quantify satellite cells on muscle sections (Hindi and Kumar, 2016; Ogura et al., 2015). Transverse sections generated from uninjured and 5d-injured TA muscle of Ire1$^{fl/fl}$ and Ire1^{mko} mice were immunostained for Pax7 to detect satellite cells. In addition, the sections were immunostained for laminin to mark the boundary of the myofibers and DAPI was used to stain nuclei (**Figure 3A**). There was no significant difference in the number of satellite cells in uninjured TA muscle of Ire1$^{fl/fl}$ and Ire1^{mko} mice (**Figure 3A**). However, the number of satellite cells per unit area was significantly reduced in injured TA muscle of Ire1^{mko} mice compared with injured TA muscle of Ire1$^{fl/fl}$ mice (**Figure 3A, 3B**). Moreover, mRNA levels of Pax7 were found to be significantly reduced in injured TA muscle of Ire1^{mko} mice compared to that of Ire1$^{fl/fl}$ mice (**Figure 3C**). Similarly, protein levels of Pax7 were also markedly lower in 5d-injured TA muscle of Ire1^{mko} mice compared with Ire1$^{fl/fl}$ mice (**Figure 3D**).

Fluorescence-activated cell sorting (FACS) analysis using a combination of cell surface markers (i.e. CD45^{-}, CD31^{-}, Ter119^{-}, Sca-1^{-}, and α7-β1 Integrin^{+}) is another approach to quantify the number of satellite cells in skeletal muscle in mice (Hindi and Kumar, 2016; Ogura et al., 2015). We next performed FACS to quantify the number of satellite cells in skeletal muscle of Ire1$^{fl/fl}$ and Ire1^{mko} mice. There was no significant difference in the numbers of satellite cells between uninjured TA muscle of Ire1$^{fl/fl}$ and Ire1^{mko} mice (data not shown). However, our analysis showed that proportion of satellite cells was significantly reduced in the 5d-injured TA muscle of Ire1^{mko} mice compared to injured TA muscle of Ire1$^{fl/fl}$ mice (**Figure 3E, 3F**). Collectively, these results suggest that myofiber-specific ablation of IRE1α reduces the number of satellite cells in injured muscle microenvironment.

Targeted ablation of IRE1 reduces proliferation of satellite cells in injured muscle. Using EdU labelling for proliferating cells, we sought to investigate whether myofiber-specific deletion of IRE1α affects satellite cell proliferation in a cell non-autonomous manner. TA muscle of $Ire1^{fl/fl}$ and $Ire1^{mKO}$ mice were injured by intramuscular injection of 1.2% $BaCl_2$ solution. After 72 h, the mice were given a single intraperitoneal injection of EdU and the TA muscle was isolated 11 days later, and stained for the detection of EdU^+ myonuclei. The boundaries of myofibers were identified by staining for laminin protein whereas nuclei were counterstained using DAPI (**Figure 4A**). Intriguingly, we found that that the number of EdU^+ nuclei per myofiber was significantly reduced in TA muscle of $Ire1^{mko}$ mice compared with corresponding $Ire1^{fl/fl}$ mice (**Figure 4B**). Moreover, the proportion of myofibers containing two or more EdU^+ centrally located nuclei was significantly reduced in $Ire1^{mko}$ mice compared with $Ire1^{fl/fl}$ mice (**Figure 4C**). These results suggest that myofiber-specific deletion of IRE1α reduces proliferation and fusion of satellite cells with injured myofibers during muscle regeneration.

We also studied whether IRE1α influences the self-renewal or differentiation of satellite cells in a cell non-autonomous manner. We employed a suspension culture of EDL myofiber explants that represents an *ex vivo* model representing muscle injury *in vivo* with respect to the activation, proliferation, and differentiation of satellite cells (Hindi and Kumar, 2016; Xiong et al., 2017). In this system, each freshly isolated myofiber is associated with a fixed number quiescent ($Pax7^+/MyoD^-$) satellite cells. About 24h in cultures, satellite cells upregulate MyoD ($Pax7^+/MyoD^+$) and start proliferating to form cell aggregates on myofibers. Cells on cultured myofiber then either terminally differentiate ($Pax7^-/MyoD^+$) or undergo self-renewal ($Pax7^+/MyoD^-$) and enter quiescence (Hindi and Kumar, 2016; Ogura et al., 2015). Immunostaining of freshly isolated myofibers from EDL muscle of $Ire1^{fl/fl}$ and $Ire1^{mko}$ mice showed no significant difference in the numbers of ($Pax7^+/MyoD^-$) cells and with undetectable levels of MyoD expression (data not shown). After 72h in suspension culture, the number of clusters per myofiber and number of cells per cluster were found to be significantly reduced in myofiber cultures prepared from $Ire1^{mKO}$ mice compared with $Ire1^{fl/fl}$ mice (**Figure 4D-F**). Our analysis also showed that there was a significant decrease in number of self-renewing ($Pax7^+/MyoD^-$), proliferating ($Pax7^+/MyoD^+$), and differentiating ($Pax7^-/MyoD^+$) satellite cells per myofiber in $Ire1^{fl/fl}$ cultures compared to $Ire1^{mko}$ mice (**Figure 4G-I**) suggesting that deletion of IRE1α in myofiber reduces the overall pool of satellite cells without influencing their self-

renewal, proliferation, or differentiation properties. To directly investigate the role of IRE1α in the proliferation of myofiber-associated satellite cells, we pulse-labelled satellite cells with EdU followed by immunostaining for Pax7 and detection of EdU (**Supplemental Figure S1**). Results showed that the number of $Pax7^{+}/EdU^{+}$ satellite cells per cluster was significantly reduced in $Ire1^{mKO}$ mice compared with $Ire1^{fl/fl}$ mice (**Figure 4J**).

IRE1α improves skeletal muscle regeneration through XBP1. IRE1α is an endonuclease that causes the alternative splicing of XBP1 mRNA to generate a transcriptionally active XBP1 (sXBP1). In addition, IRE1α activation can cause the cleavage of other ER-localized mRNAs, cytosolic mRNAs, and microRNAs, leading to their degradation through a process named RIDD (Hollien and Weissman, 2006; Maurel et al., 2014). By performing qPCR, we first compared the levels of various mRNAs that are known to be degraded by RIDD process in uninjured and injured TA muscle of $Ire1^{fl/fl}$ and $Ire1^{mKO}$ mice. Results showed that there was no significant difference in mRNA levels of known RIDD targets such as Bloc1S1, Hgsnat, ERdj4, Col6, Pdqfrb, Scara3, and Sparc in uninjured or 5d-injured TA muscle of $Ire1^{fl/fl}$ and $Ire1^{mKO}$ mice. A recent study showed that IRE1α reduces the levels myostatin in muscle cells through RIDD (He et al., 2021). However, we did not find any significant difference in mRNA levels of myostatin between uninjured or 5d-injured TA muscle of $Ire1^{fl/fl}$ and $Ire1^{mKO}$ mice (**Supplementary Figure S2**). By contrast, mRNA levels of sXBP1 were found to be drastically reduced in TA muscle of $Ire1^{mKO}$ mice compared with $Ire1^{fl/fl}$ mice (**Figure S2A**).

To understand whether IRE1α promotes satellite cell proliferation and skeletal muscle regeneration in adult mice through activating XBP1 transcription factor, we crossed floxed Xbp1 ($Xbp1^{fl/fl}$) mice with MCK-Cre line to generate muscle-specific Xbp1-knockout ($Xbp1^{mKO}$) and littermate $Xbp1^{fl/fl}$ mice. There is a drastic reduction in the levels of both unspliced XBP1 and sXBP1 in skeletal muscle of $Xbp1^{mKO}$ mice compared with littermate $Xbp1^{fl/fl}$ mice, as described (Bohnert et al., 2019; Parveen et al., 2021). Finally, TA muscle of littermate $Xbp1^{fl/fl}$ and $Xbp1^{mKO}$ mice was injured through intramuscular injection of 1.2% $BaCl_2$ solution and muscle regeneration was studied at day 5 and 14 days post-injury. H&E staining of TA muscle sections showed that there was a considerable reduction in the regeneration of TA muscle of $Xbp1^{mKO}$ mice compared to $Xbp1^{fl/fl}$ mice (**Figure 5A**). Morphometric analysis also showed that there was a significant decrease in the average myofiber CSA and Minimal Feret's diameter and proportion

of myofibers containing two or more centrally located nuclei in 5d-injured TA muscle of $Xbp1^{mKO}$ mice compared with $Xbp1^{fl/fl}$ mice (**Figure 5B-D**). Moreover, the size of the regenerating myofibers was also found to be significantly reduced in 14d-injured TA muscle of $Xbp1^{mKO}$ mice compared with $Xbp1^{fl/fl}$ mice (**Figure 5A, 5E, 5F**).

By performing immunostaining for Pax7 protein, we also quantified the number of satellite cells in $Xbp1^{fl/fl}$ and $Xbp1^{mKO}$ mice. There was no significant difference in the number of $Pax7^{+}$ cells in uninjured TA muscle of $Xbp1^{fl/fl}$ and $Xbp1^{mKO}$ mice (data not shown). However, the number of satellite cells was found to be significantly reduced in 5d-injured TA muscle of $Xbp1^{mKO}$ mice compared with $Xbp1^{fl/fl}$ mice (**Figure 5G, H**). Moreover, mRNA levels of Pax7 were also found to be significantly reduced in 5d-injured TA muscle of $Xbp1^{mKO}$ mice compared with $Xbp1^{fl/fl}$ mice (**Figure 5I**). Taken together, these results suggest that IRE1α promotes skeletal muscle regeneration through the activation of XBP1 transcription factor.

IRE1α regulates Notch signaling in injured muscle microenvironment. To understand the mechanisms by which IRE1α-mediated signaling promotes proliferation of satellite cells, we first studied the gene expression of insulin growth factor-1 (IGF1), fibroblast growth factor (FGF) 1 and 2, hepatocyte growth factor (HGF), and stromal-derived factor 1 (SDF1) which are known to promote satellite cell proliferation (Yin et al., 2013). We found no significant difference in mRNA levels of IGF1, FGF1, HGF, or SDF1 in 5d-injured TA muscle of $Ire1^{fl/fl}$ and $Ire1^{mKO}$ mice. There was a small but significant increase in mRNA levels of FGF2 in 5d-injured muscle of $Ire1^{mKO}$ mice compared with littermate $Ire1^{fl/fl}$ mice (**Supplemental Figure S3**).

Several studies have demonstrated that Notch signaling is essential for the self-renewal and proliferation of satellite cells during regenerative myogenesis. To further understand the potential mechanisms through which IRE1α signaling in myofibers regulate satellite cell proliferation and skeletal muscle regeneration, we first measured mRNA levels of Notch ligands (Jagged1, Jagged2, DLL1 and DLL4), Notch receptors (Notch1, Notch2, and Notch3) and target genes (Hes1, Hes6, Hey1 and HeyL) by qPCR assay. Interestingly, mRNA levels of Notch1, Notch2, Notch3, Jagged1, Jagged2, Hes6, Hey1, and HeyL were found to be significantly reduced in 5d-injured TA muscle of $Ire1^{mko}$ mice compared with $Ire1^{fl/fl}$ mice (**Figure 6A-C)**. Western blot analysis also showed that the protein levels of Notch1 and Hes6 were considerably reduced in injured TA muscle of $Ire1^{mKO}$ mice compared with $Ire1^{fl/fl}$ mice (**Figure 6D**). These

results suggest that myofiber-specific ablation of IRE1α reduces the activation of Notch signaling during skeletal muscle regeneration.

Wnt signaling also plays an important role during skeletal muscle regeneration. The levels of various Wnt ligands and receptors are increased in skeletal muscle upon injury. Moreover, Wnt signaling has been found to promote myoblast fusion both *in vivo* and *in vitro*. We investigated whether targeted ablation of IRE1α influences the activation of Wnt pathway during skeletal muscle regeneration. However, we found no significant difference in the gene expression of Wnt ligands Wnt4, Wnt5a, Wnt7a and Wnt11, Wnt receptors Frizzled (Fzd) 1, Fzd2, Fzd4 and Fzd6, and Wnt target gene Axin-2 (**Figure 6E-G**). These results suggest that IRE1α specifically regulate Notch signaling to promote satellite cell proliferation.

IRE1α regulates NF-κB signaling in regenerating skeletal muscle. NF-κB is a major transcription factor that regulates the expression of a plethora of molecules involved in cell proliferation, survival, and differentiation and inflammatory response (Hayden and Ghosh, 2004; Razani et al., 2011). NF-κB signaling has also been found to play an important role in skeletal muscle regeneration. By performing western blot, we first measured levels of phosphorylated and total p65 protein (a marker for activation of canonical NF-κB signaling). A drastic increase in the levels of both phosphorylated p65 (p-p65) and total p65 was observed in 5d-injured TA muscle of both $Ire1^{fl/fl}$ and $Ire1^{mKO}$ mice. However, the levels of p-p65 protein were found to be significantly reduced in 5d-injured TA muscle of $Ire1^{mKO}$ mice compared with $Ire1^{fl/fl}$ mice (**Figure 7A, 7B**). We also measured the levels of p100 and p52, the markers of activation of non-canonical NF-kB signaling pathway. Muscle injury drastically increased the levels of p100 and p52 protein in TA muscle of both $Ire1^{fl/fl}$ and $Ire1^{mKO}$ mice. Intriguingly, protein levels of both p100 and p52 were found to be significantly higher in injured TA muscle of $Ire1^{mKO}$ mice compared with $Ire1^{fl/fl}$ mice (**Figure 7A, 7C**).

We also measured mRNA levels of a few cytokines that regulate myogenesis. Our qPCR analysis showed that mRNA levels of TNF-α, TNF receptor (TNFR) 2, and TWEAK receptor Fn14 were found to be significantly reduced in injured TA muscle of $Ire1^{mKO}$ mice compared with $Ire1^{fl/fl}$ mice (**Figure 7D**). By contrast, mRNA levels of IL-4 and IL-10 were significantly increased in injured TA muscle of $Ire1^{mKO}$ mice compared to $Ire1^{fl/fl}$ mice. There was no significant difference in the mRNA levels of TNFR1, TWEAK, and IL-6 between injured muscle

of Ire1$^{fl/fl}$ and Ire1^{mKO} mice (**Figure 7D**). Taken together, these results suggest that myofiber-specific ablation of IRE1α influences the activation of canonical and non-canonical NF-κB pathways and regulates the expression of key cytokines and their receptors during regenerative myogenesis.

Myofiber-specific deletion of IRE1 exacerbates dystrophic phenotype in mdx mice. DMD, the most common X-linked lethal disorder, is caused by loss of dystrophin, a cytoskeletal protein, which provides mechanical reinforcement to the sarcolemma (Emery, 1998; Hoffman et al., 1987). Dystrophin-deficient myofibers undergo chronic muscle injury and regeneration. The mdx mouse, which lacks dystrophin protein due to a mutation that results in a premature stop codon in exon 23, is widely used as a mouse model for studying chronic muscle injury and pathophysiology of DMD (Chang et al., 2016; Shin et al., 2013). Thus, we employed mdx mice to evaluate the role of IRE1α in muscle regeneration in the "settings" of chronic muscle injury and myopathy.

We first investigated how IRE1/XBP1α pathway is affected in skeletal muscle of mdx mice. Results showed that the levels of phosphorylated IRE1α (p-IRE1α) was significantly increased whereas total IRE1α protein was significantly reduced in skeletal muscle of mdx mice compared to corresponding control mice. Indeed, the ratio of phosphorylated versus total IRE1α as well as levels of sXBP1 protein were significantly higher in skeletal muscle of mdx mice compared with control mice (**Figure 8A, 8B**) suggesting activation of IRE1α/XBP1 pathway in dystrophic muscle of mdx mice. To understand the role of IRE1α in regeneration of dystrophic muscle, we crossed Ire1^{mKO} mice with mdx mice to generate littermate mdx;Ire1$^{fl/fl}$ and mdx;Ire1^{mKO} mice. There was no significant difference in the body weight of 12-week old littermate mdx;Ire1$^{fl/fl}$ and mdx;Ire1^{mKO} mice (**Figure 8C**). However, there was a significant reduction in four paw grip strength (normalized with body weight) of mdx;Ire1^{mKO} mice compared with mdx;Ire1$^{fl/fl}$ mice (**Figure 8D**). We next isolated hind limb muscle from these mice and performed H&E staining (**Figure 8E**). Interestingly, our results showed that average CSA of the regenerating myofiber (centronucleated) was significantly reduced in TA muscle of mdx;Ire1^{mKO} mice compared to mdx;Ire1$^{fl/fl}$ mice (**Figure 8E, 8F**). Furthermore, there was a significant reduction in number of myofibers containing two or more centrally located nuclei in mdx;Ire1^{mKO} mice compared with mdx;Ire1$^{fl/fl}$ mice (**Figure 8G**). Similarly, muscle regeneration

was also considerably reduced in GA muscle of Ire1^{mKO} mice compared with mdx;Ire1$^{fl/fl}$ mice (**Supplemental Figure S4A, S4B**). We also investigated how myofiber-specific deletion of IRE1α affects the frequency of satellite cells in dystrophic muscle of mdx mice. TA muscle sections generated from littermate mdx;Ire1$^{fl/fl}$ and mdx;Ire1^{mKO} mice were immunostained for Pax7 and laminin whereas nuclei were counterstained with DAPI. Finally, the number of Pax7^{+} cells within laminin staining was counted. Results showed that frequency of satellite cells per myofiber was significantly reduced in TA muscle of mdx;Ire1^{mKO} mice compared with mdx;Ire1$^{fl/fl}$ mice (**Figure 8H, 8I**). There was also a significant reduction in the mRNA levels of Pax7 in TA muscle of mdx;Ire1^{mKO} mice compared with mdx;Ire1$^{fl/fl}$ mice (**Figure 8J**). Finally, our qPCR analysis showed that there was no significant difference in mRNA levels Bloc1S1 or myostatin in dystrophic muscle of mdx;Ire1$^{fl/fl}$ and mdx;Ire1^{mKO} mice (Supplemental Figure S4C). By contrast, mRNA levels of Notch targets Hes1, Hey1, and HeyL were found to be significantly reduced in skeletal muscle of mdx;Ire1^{mKO} mice compared with mdx;Ire1$^{fl/fl}$ mice (**Supplemental Figure S4D**). These results further suggest that Ire1α improves muscle regeneration through augmenting satellite cell proliferation in response to acute injury and in dystrophic muscle of mice.

Discussion

Skeletal muscle repair in response to injury is regulated by multiple factors produced by damaged myofibers, satellite stem cells, and several other cell types that are either resident in the muscle or recruited to assist in clearing cellular debris and support regeneration (Yin et al., 2013). Furthermore, it is now increasingly clear that several signaling pathways are activated in injured myofibers that regulate specific steps of muscle regenerative program in adults (Brack and Munoz-Canoves, 2016; Dumont et al., 2015). Recent studies have provided evidence that many catabolic stimuli including muscle injury lead to the activation of ER stress-induced UPR pathways in skeletal muscle (Afroze and Kumar, 2019; Bohnert et al., 2018; Miyake et al., 2016; Xiong et al., 2017). In the present study, we demonstrate that muscle injury leads to the activation of IRE1/XBP1 signaling axis in skeletal muscle and that deletion of IRE1 or XBP1 in myofibers attenuate skeletal muscle regeneration potentially through inhibiting the proliferation of satellite cells in cell non-autonomous manner. Our study also demonstrates that IRE1-

mediated signaling in myofiber is essential for the regeneration of injured myofibers in dystrophic muscles of mdx mice.

Skeletal muscle regeneration is accomplished through the activation of satellite cells which proliferate and differentiate to become myoblasts that eventually fuse with injured myofibers to complete regeneration (Kuang and Rudnicki, 2008; Yin et al., 2013). While the frequency of satellite cells in skeletal muscle of healthy individuals remain constant, their number and regenerative potential can be altered in various disease states and conditions (Brack and Munoz-Canoves, 2016; Dumont et al., 2015). We found that ablation of IRE1α in myofibers has no noticeable effect on skeletal muscle development or myofiber size in mice. Furthermore, genetic ablation of IRE1α in differentiated myofibers does not influence the frequency of satellite cells in naïve conditions (Figure 3). In contrast, myofiber-specific deletion of IRE1α inhibits the regeneration of skeletal muscle in response to injury in adult mice. Our results also demonstrate that the size of the regenerating myofibers and levels of various MRFs such as Myf5, MyoD and myogenin as well as eMyHC are considerably reduced in injured muscle of $Ire1^{mKO}$ mice (**Figure 2**) suggesting that IRE1α-mediated signaling supports the early steps of muscle regenerative program.

IRE1α, the most evolutionary conserved UPR signaling branch, is a serine/threonine protein kinase and endoribonuclease that cleave and initiate splicing of the XBP1 mRNA (Tabas and Ron, 2011; Walter and Ron, 2011). Activated IRE1α endoribonuclease removes 26-nucleotide intron from XBP1, resulting in a translational frame-shift to modify unspliced XBP1 into spliced XBP1 transcription factor that enforces adaptive programs (Hetz, 2012; Walter and Ron, 2011; Wang and Kaufman, 2014). Activated IRE1α also controls various biological processes, including cell death and inflammation through degradation of a subset of mRNAs and microRNAs through a process known as RIDD (Hollien and Weissman, 2006; Maurel et al., 2014). The target mRNAs of RIDD in mammalian cells require a consensus motif of 5′-CUGCAG-3′, along with a secondary stem loop structure. The disruption in stem loop formation or mutation in the consensus sequence hampers RIDD-mediated degradation of the target mRNA (Bright et al., 2015; Oikawa et al., 2010). Intriguingly, in response to some stimuli, such as genotoxic stress or microbial products, IRE1α signaling is activated without any noticeable ER

stress signature (Abdullah and Ravanan, 2018; Dufey et al., 2020; Martinon et al., 2010). For example, in response to DNA damage in fibroblasts, IRE1α signaling is activated in the absence of an ER stress leading to the activation of RIDD process without having any effect on XBP1 mRNA splicing (Dufey et al., 2020). There is also a recent report suggesting that IRE1α promotes skeletal muscle regeneration through reducing the levels of myostatin via RIDD mechanism (He et al., 2021). Although we have used different floxed IRE1 line and we employed MCK-Cre line to ablate IRE1α in myofibers, we did not find any significant difference in the levels of myostatin in uninjured or injured muscle of $Ire1^{fl/fl}$ and $Ire1^{mko}$ mice (**Figure S2**). In addition, we also did not find any difference in other known mRNAs which are degraded through RIDD-dependent mechanisms suggesting that IRE1α may not be regulating myofiber regeneration through RIDD pathway (**Figure S2)**. These results are consistent with the findings that RIDD-dependent mRNA decay occurs only when there is an ectopic activation of IRE1α with concomitant inhibition of protein synthesis (Moore and Hollien, 2015). Indeed, our results demonstrating that myofiber-specific ablation of XBP1 using the same MCK-Cre line produces similar effects as that of IRE1α (**Figure 5**) suggest that IRE1α promotes skeletal muscle regeneration through activating its canonical output mediated by the transcription factor XBP1.

Strikingly, our results demonstrate that genetic ablation of IRE1 or XBP1 in myofibers significantly reduces the proliferation of satellite cells without having any significant impact on their self-renewal, survival, or differentiation (**Figures 3, 4, 5**). Notch signaling is quite unique that it can regulate the fate of one cell with that of a cellular neighbor through interaction between the Notch receptor and the membrane-bound Notch ligands that are expressed in a juxtaposed cell (Kann et al., 2021). It is now evidenced that the outcome of Notch signaling is dependent on the cellular context and is capable of influencing quiescence, self-renewal, survival, and differentiation cell fates. Notch signaling has also been shown to regulate the self-renewal and proliferation of satellite stem cells both *in vivo* and *in vitro* (Bi et al., 2016; Kann et al., 2021; Vasyutina et al., 2007). Interestingly, our results demonstrate that levels of Notch receptor 1, 2 and 3 and Notch ligands Jagged1 and Jagged2 are significantly reduced in injured muscle of $Ire1^{mKO}$ mice compared with $Ire1^{fl/fl}$ mice. In addition, transcript levels of Notch target genes are also reduced in regenerating muscle of $Ire1^{mKO}$ mice further suggesting an inhibition in Notch signaling upon myofiber-specific ablation of IRE1α (**Figure 6**). Previous studies have also

shown that the levels of various components of canonical Wnt signaling are increased in injured skeletal muscle and Wnt signaling promotes myoblast fusion during regenerative myogenesis (Hindi et al., 2017; Hindi et al., 2013). Indeed, spatial activation of Notch and Wnt signaling is important for progression of muscle regeneration upon injury (Brack et al., 2008). However, there was no significant difference in the expression of various components of Wnt signaling in regenerating muscle of $Ire1^{fl/fl}$ and $Ire1^{mko}$ mice (**Figure 6**) suggesting that IRE1α specifically regulates Notch signaling and inhibition of Notch signaling may be one of the important mechanisms for the reduced proliferation of satellite cells in $Ire1^{mKO}$ mice.

NF-κB is a major signaling pathway that regulates the expression of a number of inflammatory cytokines and growth factors. Activation of NF-κB also promotes proliferation and survival of a number of cell types. NF-κB can be activated through a canonical pathway that involves the activation of IKKβ and p65 subunits. In non-canonical pathway, protein levels of NIK are increased due to inhibition of its degradation. NIK phosphorylates IKKα which in turn phosphorylates p100 protein leading to its proteolytic processing into p52 subunit (Hayden and Ghosh, 2004; Razani et al., 2011). Accumulating evidence suggests that canonical NF-κB signaling is activated at initial stages of myogenesis to augment the proliferation of muscle progenitor cells (Li et al., 2008; Straughn et al., 2019). In contrast, non-canonical NF-κB signaling augments myoblast fusion during myogenesis (Enwere et al., 2012; Hindi et al., 2017; Hindi et al., 2013). Interestingly, our results suggest that the levels of phosphorylated p65 protein as well as gene expression of TNFα, a potent inducer of canonical NF-κB signaling (Hayden and Ghosh, 2004), are significantly reduced in regenerating myofibers of $Ire1^{mko}$ mice compared to $Ire1^{fl/fl}$ mice. In contrast, there was a significant increase in the levels of p100 and p52 proteins in the injured muscle of $Ire1^{mko}$ mice compared to $Ire1^{fl/fl}$ mice suggesting activation of non-canonical NF-κB signaling upon deletion of IRE1α (**Figure 7**). Although the physiological significance of differential activation of canonical and non-canonical NF-κB pathway remains unknown, it is possible that inhibition of canonical signaling is another mechanism for the reduced proliferation of satellite cells in injured skeletal muscle of $Ire1^{mKO}$ mice. Alternatively, spurious activation of non-canonical NF-κB signaling may cause precautious fusion of muscle progenitor cells leading to deficits in muscle regeneration.

DMD is a genetic muscle disorder which involves chronic degeneration and regeneration of myofibers (Emery, 1998). It has been postulated that inadequate muscle regeneration in DMD is due to exhaustion of satellite cells after several rounds of myofiber degeneration and regeneration (Chang et al., 2016). In contrast to DMD patients, skeletal muscles of mdx mice maintain their ability to regenerate throughout life. Indeed, mdx mice serve as an excellent model to study muscle regeneration in disease conditions and in response to chronic myofiber injury (Blake et al., 2002; Chang et al., 2016; Shin et al., 2013). Our results demonstrate that genetic ablation of IRE1α exacerbates dystrophic phenotype and reduces the proportion of regenerating myofibers in skeletal muscle mdx mice (**Figure 8**). These results are consistent with the recently published report demonstrating that myoblast-specific deletion of IRE1α also exacerbates dystrophic phenotype in mdx mice (He et al., 2021). In contrast to this published report (He et al., 2021), we did not find any significant difference in the levels of myostatin or Bloc1S1 suggesting that IRE1α does not influence RIDD process in dystrophic muscle of mdx mice. Interestingly, our analysis also showed that myofiber-specific deletion of IRE1α significantly reduced the number of satellite cells (**Figure 8**) and gene expression of Notch targets in skeletal muscle of mdx mice (**Figure S4C**) further suggesting that IRE1α signaling in myofibers promotes proliferation of satellite cells to support muscle regeneration.

In summary, our study provides initial evidence that IRE1/XBP1 signaling in myofibers is activated during acute or chronic muscle injury and its main function is to promote muscle regeneration through augmenting proliferation of satellite cells in a cell non-autonomous manner. Future studies will investigate the cell-autonomous role of satellite cells and whether augmenting IRE1α/XBP1 signaling can improve muscle regeneration in various muscle degenerative disorders.

Materials and Methods

Animals. C57BL/6 mice and mdx (strain: C57BL/10ScSn-^{Dmdmdx}/J) mice were purchased from Jackson Laboratories (Bar Harbor, ME, USA) and breeding colonies were maintained at the University of Houston animal resource facility. Floxed Ire1 (Ire1$^{fl/fl}$) mice as described (Iwawaki et al., 2009) were crossed with MCK-Cre mice (Jax strain: B6.FVB(129S4)-Tg (Ckmm-

cre)5Khn/J) to generate muscle-specific IRE1α-knockout (i.e. $Ire1^{mKO}$) mice. $Ire1^{mKO}$ mice were also crossed with mdx mice to generate littermate mdx;$Ire1^{fl/fl}$ and mdx;$Ire1^{mKO}$ mice. Skeletal muscle specific XBP1-knockout mice ($Xbp1^{mKO}$) mice were generated by crossing $Xbp1^{fl/fl}$ (MGI strain: $Xbp1^{tm2Glm}$) mice as described (Hetz, 2012) with MCK-Cre mice. All mice were in the C57BL6 background and their genotype was determined by PCR from tail DNA. All the experiments were performed in strict accordance with the recommendations in the Guide for the Care and Use of Laboratory Animals of the National Institutes of Health. All of the animals were handled according to approved institutional animal care and use committee (IACUC) protocols of the University of Houston. All surgeries were performed under anesthesia, and every effort was made to minimize suffering.

Grip strength measurements. To measure total four-limb grip strength of mice, a digital grip-strength meter (Columbus Instruments, Columbus, OH, USA) was used. In brief, the mice were acclimatized for 5 min and then allowed to grab the metal pull bar with all four paws. The mouse tail was then gently pulled backward in the horizontal plane until it could no longer grasp the bar. The force at the time of release was recorded as the peak tension. Each mouse was tested five times with a 1 min break between tests. The average peak tension from five attempts normalized against total body weight was defined as grip strength.

Skeletal muscle injury and *in vivo* fusion assay. Muscle necrotic injury in adult mice was performed by injection of 50 µl of 1.2% $BaCl_2$ (Sigma Chemical Co.) dissolved in saline into the TA muscle as described (Hindi and Kumar, 2016; Hindi et al., 2012). At various time points after intramuscular injection of $BaCl_2$, the mice were euthanized and TA muscle was collected for biochemical and histological studies. To study myoblast fusion *in vivo*, the mice were given an intraperitoneal injection of EdU (4 µg per gram body weight) at day 3 after intramuscular injection of 1.2% $BaCl_2$ into the TA muscle. After 11 days of EdU injection, the TA muscle was isolated and sectioned in a microtome cryostat. The sections were subsequently immunostained with anti-Laminin, DAPI for the detection of nuclei, and processed for the detection of EdU similar to as described (Hindi et al., 2017). Finally, the number of intramyofiber EdU^+ myonuclei/myofiber was quantified using NIH ImageJ software.

Histology and morphometric analysis. Uninjured and injured TA muscles were isolated from mice, snap frozen in liquid nitrogen, and sectioned with a microtome cryostat. For the assessment of muscle morphology and to quantify fiber cross-sectional area (CSA), 10μm thick transverse sections of TA muscle were stained with hematoxylin and eosin (H&E). The sections were examined under an Eclipse TE 2000-U microscope (Nikon, Tokyo, Japan). For quantitative analysis, cross-sectional area (CSA) and minimal Feret's diameter of myofibers was analyzed in H&E-stained TA muscle sections using Nikon NIS Elements BR 3.00 software (Nikon). For each muscle, the distribution of fiber CSA was calculated by analyzing approximately 300 myofibers. Masson's Trichrome staining was performed to analyze fibrosis using a commercially available kit and following a protocol suggested by the manufacturer (Richard-Allan Scientific).

Isolation and culturing of myofiber. Single myofiber cultures were established from EDL muscle after digestion with collagenase II (Worthington Biochemical Corporation, Lakewood, NJ) and trituration as described (Hindi and Kumar, 2016). Suspended myofibers were cultured in 60 mm horse serum-coated plates in Dulbecco's modified Eagle's medium (DMEM) supplemented with 10% fetal bovine serum (FBS; Invitrogen), 2% chicken embryo extract (Accurate Chemical, Westbury, NY), 10 ng/ml basis fibroblast growth factor (Peprotech, Rocky Hill, NJ), and 1% penicillin-streptomycin for three days.

Immunofluorescence. For the immunohistochemistry studies, frozen TA muscle sections or myofiber were fixed in 4% paraformaldehyde (PFA) in PBS, blocked in 2% bovine serum albumin in PBS for 1 hr and incubated with anti-Pax7 (1:10, DSHB Cat# pax7, RRID:AB_528428), anti-eMyHC (1:200, DSHB Cat# F1.652 RRID:AB_528358), anti-laminin (1:500, Sigma-Aldrich Cat# L9393 RRID:AB_477163), or anti-MyoD (1:200, Santa Cruz Biotechnology Cat# sc-304 RRID:AB_631992) in blocking solution at 4°C overnight under humidified conditions. The sections were washed briefly with PBS before incubation with Alexa Fluor 488 (Thermo Fisher Scientific Cat# A-11034 also A11034 RRID:AB_2576217) or Alexa Fluor 594 (Thermo Fisher Scientific Cat# A-11037 also A11037 RRID:AB_2534095) secondary antibody for 1 hr at room temperature and then washed 3 times for 5 min with PBS. The slides were mounted using fluorescence medium (Vector Laboratories) and visualized at room temperature on Nikon Eclipse TE 2000-U microscope (Nikon), a digital camera (Nikon Digital

Sight DS-Fi1), and Nikon NIS Elements BR 3.00 software (Nikon). Image levels were equally adjusted using Abode Photoshop CS6 software (Adobe).

Fluorescence-activated cell sorting (FACS). Satellite cells were analyzed by performing FACS analysis as described (Hindi and Kumar, 2016). For satellite cell isolation from heterogeneous cell population, cells were immunostained with antibodies against CD45, CD31, Sca-1, and Ter-119 for negative selection (all PE conjugated, ThermoFisher), and with α7-integrin (MBL International) for positive selection. Alexa Fluor 488 goat anti-mouse (ThermoFisher, Cat# A-11029 also A11029 RRID:AB_138404) was used as a secondary antibody against α7-integrin.

Total RNA extraction and qPCR assay. RNA isolation and qPCR were performed using similar protocol as described (Paul et al., 2012; Paul et al., 2010). In brief, total RNA was extracted from uninjured and injured TA muscle of mice using TRIzol reagent (ThermoFisher Scientific) and an RNeasy Mini Kit (Qiagen, Valencia, CA, USA) according to the manufacturers' protocols. First-strand cDNA for PCR analyses was made with a commercially available kit (iScript™ cDNA Synthesis Kit, Bio-Rad Laboratories). The quantification of mRNA expression was performed using the SYBR Green dye (Bio-Rad SsoAdvanced™ - Universal SYBR® Green Supermix) method on a sequence detection system (CFX384 Touch Real-Time PCR Detection System - Bio-Rad Laboratories). Primers were designed with Vector NTI software (Thermo Fisher Scientific Life Sciences) and are available from the authors on request. Data normalization was accomplished with the endogenous control (β-actin), and the normalized values were subjected to a $2^{-\Delta\Delta Ct}$ formula to calculate the fold change between control and experimental groups.

Western blot analysis. Estimation of the presence of various proteins was quantitated by performing Western blot analysis as described (Hindi and Kumar, 2016; Ogura et al., 2015). TA muscle of mice were washed with sterile PBS and homogenized in lysis buffer: 50 mM Tris-Cl (pH 8.0), 200 mM NaCl, 50 mM NaF, 1 mM dithiothreitol, 1 mM sodium orthovanadate, 0.3% IGEPAL, and protease inhibitors. Approximately 100 μg protein was resolved in each lane on 10% SDS-polyacrylamide gels, electrotransferred onto nitrocellulose membranes, and probed with the following antibodies: anti-phospho-IRE1α (1:500; Novus, NB 100-2323), anti-IRE1α

(1:500; Cell Signaling Technology, #3294), anti-sXBP-1 (1:1000; Cell Signaling Technology, #12782), anti-Pax7 (1:100; DSHB Cat# pax7, RRID:AB_528428), anti-eMyHC (1:200, DSHB Cat# F1.652 RRID:AB_528358), anti-MyoD (Santa Cruz Biotechnology), anti-Myogenin (1:100; DSHB Cat# F5D), anti-phospho-p65 (1:500; Cell Signaling Technology, #3033), anti-p65 (1:500; Cell Signaling Technology, # 8242), anti-p100/p52 (1:500; Cell Signaling Technology, #4882), anti-Notch1 (Santa Cruz Biotechnology, #SC-6015), anti-Hes6 (Santa Cruz Biotechnology, #SC-25396), and anti-GAPDH (1:2000; Cell Signaling Technology, #2118). Antibodies were detected by chemi-luminescence. Quantitative estimation of the bands' intensity was performed with ImageJ software (NIH).

Statistical analysis. Results are expressed as means ± SEM. For statistical analysis, we used paired Student's t test or analysis of variance (ANOVA) followed by Tukey's multiple comparison test to compare quantitative data.

ACKNOWLEDGMENTS. We thank Dr. Laurie Glimcher of Cornell University for providing floxed XBP1 mice. This work was supported by funding from NIH grants AR059810 and AR068313 to AK.

AUTHORS CONTRIBUTION. AK designed the work. AR, MTS, RB, and KRB performed all the experiments and analyzed results. IW provided floxed Ire1 mice. AK and AR wrote the manuscript. All the authors edited and finalized the manuscript.

References

Abdullah, A., and P. Ravanan. 2018. The unknown face of IRE1alpha - Beyond ER stress. *Eur J Cell Biol*. 97:359-368.

Afroze, D., and A. Kumar. 2019. ER stress in skeletal muscle remodeling and myopathies. *FEBS J*. 286:379-398.

Bi, P., F. Yue, Y. Sato, S. Wirbisky, W. Liu, T. Shan, Y. Wen, D. Zhou, J. Freeman, and S. Kuang. 2016. Stage-specific effects of Notch activation during skeletal myogenesis. *Elife*. 5.

Blake, D.J., A. Weir, S.E. Newey, and K.E. Davies. 2002. Function and genetics of dystrophin and dystrophin-related proteins in muscle. *Physiological reviews*. 82:291-329.

Bohnert, K.R., P. Goli, A. Roy, A.K. Sharma, G. Xiong, Y.S. Gallot, and A. Kumar. 2019. The Toll-Like Receptor/MyD88/XBP1 Signaling Axis Mediates Skeletal Muscle Wasting during Cancer Cachexia. *Mol Cell Biol*. 39.

Bohnert, K.R., J.D. McMillan, and A. Kumar. 2018. Emerging roles of ER stress and unfolded protein response pathways in skeletal muscle health and disease. *J Cell Physiol*. 233:67-78.

Brack, A.S., I.M. Conboy, M.J. Conboy, J. Shen, and T.A. Rando. 2008. A temporal switch from notch to Wnt signaling in muscle stem cells is necessary for normal adult myogenesis. *Cell Stem Cell*. 2:50-59.

Brack, A.S., and P. Munoz-Canoves. 2016. The ins and outs of muscle stem cell aging. *Skelet Muscle*. 6:1.

Bright, M.D., D.N. Itzhak, C.P. Wardell, G.J. Morgan, and F.E. Davies. 2015. Cleavage of BLOC1S1 mRNA by IRE1 Is Sequence Specific, Temporally Separate from XBP1 Splicing, and Dispensable for Cell Viability under Acute Endoplasmic Reticulum Stress. *Mol Cell Biol*. 35:2186-2202.

Chang, N.C., F.P. Chevalier, and M.A. Rudnicki. 2016. Satellite Cells in Muscular Dystrophy - Lost in Polarity. *Trends Mol Med*. 22:479-496.

Dufey, E., J.M. Bravo-San Pedro, C. Eggers, M. Gonzalez-Quiroz, H. Urra, A.I. Sagredo, D. Sepulveda, P. Pihan, A. Carreras-Sureda, Y. Hazari, E.A. Sagredo, D. Gutierrez, C. Valls, A. Papaioannou, D. Acosta-Alvear, G. Campos, P.M. Domingos, R. Pedeux, E. Chevet, A. Alvarez, P. Godoy, P. Walter, A. Glavic, G. Kroemer, and C. Hetz. 2020. Genotoxic stress triggers the activation of IRE1alpha-dependent RNA decay to modulate the DNA damage response. *Nat Commun*. 11:2401.

Dumont, N.A., Y.X. Wang, and M.A. Rudnicki. 2015. Intrinsic and extrinsic mechanisms regulating satellite cell function. *Development*. 142:1572-1581.

Emery, A.E. 1998. The muscular dystrophies. *Bmj*. 317:991-995.

Enwere, E.K., J. Holbrook, R. Lejmi-Mrad, J. Vineham, K. Timusk, B. Sivaraj, M. Isaac, D. Uehling, R. Al-Awar, E. Lacasse, and R.G. Korneluk. 2012. TWEAK and cIAP1 Regulate Myoblast Fusion Through the Noncanonical NF-kappaB Signaling Pathway. *Sci Signal*. 5:ra75.

Harding, H.P., Y. Zhang, and D. Ron. 1999. Protein translation and folding are coupled by an endoplasmic-reticulum-resident kinase. *Nature*. 397:271-274.

Hayden, M.S., and S. Ghosh. 2004. Signaling to NF-kappaB. *Genes Dev*. 18:2195-2224.

He, S., T. Fu, Y. Yu, Q. Liang, L. Li, J. Liu, X. Zhang, Q. Zhou, Q. Guo, D. Xu, Y. Chen, X. Wang, Y. Chen, J. Liu, Z. Gan, and Y. Liu. 2021. IRE1alpha regulates skeletal muscle regeneration through Myostatin mRNA decay. *J Clin Invest*.

Hetz, C. 2012. The unfolded protein response: controlling cell fate decisions under ER stress and beyond. *Nat Rev Mol Cell Biol*. 13:89-102.

Hindi, S.M., and A. Kumar. 2016. TRAF6 regulates satellite stem cell self-renewal and function during regenerative myogenesis. *J Clin Invest*. 126:151-168.

Hindi, S.M., P.K. Paul, S. Dahiya, V. Mishra, S. Bhatnagar, S. Kuang, Y. Choi, and A. Kumar. 2012. Reciprocal interaction between TRAF6 and notch signaling regulates adult myofiber regeneration upon injury. *Molecular and cellular biology*. 32:4833-4845.

Hindi, S.M., J. Shin, Y.S. Gallot, A.R. Straughn, A. Simionescu-Bankston, L. Hindi, G. Xiong, R.P. Friedland, and A. Kumar. 2017. MyD88 promotes myoblast fusion in a cell-autonomous manner. *Nat Commun*. 8:1624.

Hindi, S.M., M.M. Tajrishi, and A. Kumar. 2013. Signaling mechanisms in mammalian myoblast fusion. *Sci Signal*. 6:re2.

Hoffman, E.P., R.H. Brown, Jr., and L.M. Kunkel. 1987. Dystrophin: the protein product of the Duchenne muscular dystrophy locus. *Cell*. 51:919-928.

Hollien, J., J.H. Lin, H. Li, N. Stevens, P. Walter, and J.S. Weissman. 2009. Regulated Ire1-dependent decay of messenger RNAs in mammalian cells. *J Cell Biol*. 186:323-331.

Hollien, J., and J.S. Weissman. 2006. Decay of endoplasmic reticulum-localized mRNAs during the unfolded protein response. *Science*. 313:104-107.

Iwawaki, T., R. Akai, S. Yamanaka, and K. Kohno. 2009. Function of IRE1 alpha in the placenta is essential for placental development and embryonic viability. *Proc Natl Acad Sci U S A*. 106:16657-16662.

Kann, A.P., M. Hung, and R.S. Krauss. 2021. Cell-cell contact and signaling in the muscle stem cell niche. *Curr Opin Cell Biol*. 73:78-83.

Kuang, S., and M.A. Rudnicki. 2008. The emerging biology of satellite cells and their therapeutic potential. *Trends Mol Med*. 14:82-91.

Li, H., S. Malhotra, and A. Kumar. 2008. Nuclear factor-kappa B signaling in skeletal muscle atrophy. *J Mol Med*. 86:1113-1126.

Martinon, F., X. Chen, A.H. Lee, and L.H. Glimcher. 2010. TLR activation of the transcription factor XBP1 regulates innate immune responses in macrophages. *Nat Immunol*. 11:411-418.

Maurel, M., E. Chevet, J. Tavernier, and S. Gerlo. 2014. Getting RIDD of RNA: IRE1 in cell fate regulation. *Trends Biochem Sci*. 39:245-254.

Miyake, M., A. Nomura, A. Ogura, K. Takehana, Y. Kitahara, K. Takahara, K. Tsugawa, C. Miyamoto, N. Miura, R. Sato, K. Kurahashi, H.P. Harding, M. Oyadomari, D. Ron, and

S. Oyadomari. 2016. Skeletal muscle-specific eukaryotic translation initiation factor 2alpha phosphorylation controls amino acid metabolism and fibroblast growth factor 21-mediated non-cell-autonomous energy metabolism. *FASEB J*. 30:798-812.

Moore, K., and J. Hollien. 2015. Ire1-mediated decay in mammalian cells relies on mRNA sequence, structure, and translational status. *Mol Biol Cell*. 26:2873-2884.

Nakanishi, K., N. Dohmae, and N. Morishima. 2007. Endoplasmic reticulum stress increases myofiber formation in vitro. *FASEB J*. 21:2994-3003.

Nakanishi, K., T. Sudo, and N. Morishima. 2005. Endoplasmic reticulum stress signaling transmitted by ATF6 mediates apoptosis during muscle development. *J Cell Biol*. 169:555-560.

Ogura, Y., S.M. Hindi, S. Sato, G. Xiong, S. Akira, and A. Kumar. 2015. TAK1 modulates satellite stem cell homeostasis and skeletal muscle repair. *Nat Commun*. 6:10123.

Oikawa, D., M. Tokuda, A. Hosoda, and T. Iwawaki. 2010. Identification of a consensus element recognized and cleaved by IRE1 alpha. *Nucleic Acids Res*. 38:6265-6273.

Parveen, A., K.R. Bohnert, M. Tomaz da Silva, Y. Wen, R. Bhat, A. Roy, and A. Kumar. 2021. MyD88-mediated signaling intercedes in neurogenic muscle atrophy through multiple mechanisms. *FASEB J*. 35:e21821.

Paul, P.K., S. Bhatnagar, V. Mishra, S. Srivastava, B.G. Darnay, Y. Choi, and A. Kumar. 2012. The E3 ubiquitin ligase TRAF6 intercedes in starvation-induced skeletal muscle atrophy through multiple mechanisms. *Mol Cell Biol*. 32:1248-1259.

Paul, P.K., S.K. Gupta, S. Bhatnagar, S.K. Panguluri, B.G. Darnay, Y. Choi, and A. Kumar. 2010. Targeted ablation of TRAF6 inhibits skeletal muscle wasting in mice. *The Journal of cell biology*. 191:1395-1411.

Preissler, S., and D. Ron. 2019. Early Events in the Endoplasmic Reticulum Unfolded Protein Response. *Cold Spring Harb Perspect Biol*. 11.

Razani, B., A.D. Reichardt, and G. Cheng. 2011. Non-canonical NF-kappaB signaling activation and regulation: principles and perspectives. *Immunol Rev*. 244:44-54.

Shin, J., M.M. Tajrishi, Y. Ogura, and A. Kumar. 2013. Wasting mechanisms in muscular dystrophy. *Int J Biochem Cell Biol*. 45:2266-2279.

Straughn, A.R., S.M. Hindi, G. Xiong, and A. Kumar. 2019. Canonical NF-kappaB signaling regulates satellite stem cell homeostasis and function during regenerative myogenesis. *J Mol Cell Biol*. 11:53-66.

Tabas, I., and D. Ron. 2011. Integrating the mechanisms of apoptosis induced by endoplasmic reticulum stress. *Nat Cell Biol*. 13:184-190.

Vasyutina, E., D.C. Lenhard, H. Wende, B. Erdmann, J.A. Epstein, and C. Birchmeier. 2007. RBP-J (Rbpsuh) is essential to maintain muscle progenitor cells and to generate satellite cells. *Proc Natl Acad Sci U S A*. 104:4443-4448.

Walter, P., and D. Ron. 2011. The unfolded protein response: from stress pathway to homeostatic regulation. *Science*. 334:1081-1086.

Wang, M., and R.J. Kaufman. 2014. The impact of the endoplasmic reticulum protein-folding environment on cancer development. *Nat Rev Cancer*. 14:581-597.

Xiong, G., S.M. Hindi, A.K. Mann, Y.S. Gallot, K.R. Bohnert, D.R. Cavener, S.R. Whittemore, and A. Kumar. 2017. The PERK arm of the unfolded protein response regulates satellite cell-mediated skeletal muscle regeneration. *Elife*. 6.

Yin, H., F. Price, and M.A. Rudnicki. 2013. Satellite cells and the muscle stem cell niche. *Physiological reviews*. 93:23-67.

Zismanov, V., V. Chichkov, V. Colangelo, S. Jamet, S. Wang, A. Syme, A.E. Koromilas, and C. Crist. 2016. Phosphorylation of eIF2alpha Is a Translational Control Mechanism Regulating Muscle Stem Cell Quiescence and Self-Renewal. *Cell Stem Cell*. 18:79-90.

Figure Legends

FIGURE 1. IRE1α is required for muscle regeneration. (**A**) Left side TA muscle of wild-type mice was injected with 50 µl of 1.2% $BaCl_2$ solution whereas contralateral TA muscle was injected with normal saline to serve as uninjured control. After 5d, the TA muscles were harvested and analyzed by performing western blotting. Representative immunoblots presented here demonstrate the levels of p-IRE1, IRE1, and sXBP1 protein in uninjured and injured TA muscle. Ponceau S staining confirmed equal loading of protein in each lane (n=4 mice per group). (**B**) Immunoblots presented here show levels of IRE1α protein in TA and soleus muscle and liver of $Ire1^{fl/fl}$ and $Ire1^{mKO}$ mice. GAPDH was used as loading control (n=3 mice per group). (**C**) Representative photomicrographs of Hematoxylin and Eosin (HE)-stained sections of TA muscles of $Ire1^{fl/fl}$ and $Ire1^{mKO}$ mice at day 0, 5, and 14 after intramuscular injection of $BaCl_2$ solution. Scale bar: 50 µm. Quantification of average myofiber (**D**) cross-sectional area (CSA) (n=9 mice per group) and (**E**) Minimal Feret's diameter in TA muscle at day 5 post-injury (n=6 mice per group). (**F**) Average myofiber CSA in TA muscle of $Ire1^{fl/fl}$ and $Ire1^{mKO}$ mice after 14 days of $BaCl_2$-mediated injury (n=3 mice per group). (**G**) Percentage of myofibers containing 2 or more centrally located nuclei in TA muscle at day 5 (n=4 mice per group) and day 14 (n=3 mice per group) after $BaCl_2$-mediated injury. After 21 days of first injury, TA muscle of $Ire1^{fl/fl}$ and $Ire1^{mKO}$ mice was again given intramuscular injection of 50 µl of 1.2% $BaCl_2$ solution, and the muscle was analyzed at day 5. Representative photomicrograph of (**H**) H&E-stained, and (**I**) trichrome-stained TA muscle sections. Scale bar: 50 µm. n=3 mice per group. Data are presented as mean ± SEM. $P \leq 0.05$, values significantly different from corresponding 5d- or 14d-injured TA muscle of $Ire1^{fl/fl}$ mice by unpaired t test.

FIGURE 2. Myofiber-specific ablation of IRE1α inhibits early markers of muscle regeneration. (**A**) Representative photomicrographs of 5d-injured TA muscle sections of $Ire1^{fl/fl}$ and $Ire1^{mKO}$ mice after immunostaining for eMyHC (red) and laminin (green) protein. Nuclei were counterstained with DAPI (blue). (**B**) Frequency distribution of $eMyHC^+$ $Laminin^+$ myofiber CSA in 5d-injured TA muscle of $Ire1^{mKO}$ and $Ire1^{fl/fl}$ mice (n=4 for $Ire1^{fl/fl}$ and n=3 for $Ire1^{mKO}$ group). (**C**) Percentage of $eMyHC^+$ myofibers with 2 or more nuclei in 5d-injured TA muscle of $Ire1^{fl/fl}$ and $Ire1^{mKO}$ mice (n=4 for $Ire1^{fl/fl}$ and n=6 for $Ire1^{mKO}$ group). Data expressed as mean ± SEM. $^*P \leq 0.05$, values significantly different from 5d-injured TA muscle of $Ire1^{fl/fl}$

mice by unpaired t test. Relative mRNA levels of (**D**) Myf5, (**E**) MyoD, (**F**) Myogenin, and (**G**) eMyHC in uninjured and 5d-injured TA muscle of Ire1$^{fl/fl}$ and Ire1^{mKO} mice. (**H**) Representative western blot showing levels of eMyHC, MyoD, Myogenin, and GAPDH in uninjured and 5d-injured TA muscle of Ire1$^{fl/fl}$ and Ire1^{mKO} mice (n=3 for Uninjured Ire1$^{fl/fl}$, n=3 for Uninjured Ire1^{mKO}, n=4 for Injured Ire1$^{fl/fl}$ and n=5 for Injured Ire1^{mKO} group). Data are presented as mean ± SEM and analyzed by one-way analysis of variance (ANOVA) followed by Tukey's multiple comparison test. *****P≤0.05, values significantly different from uninjured TA muscle of Ire1$^{fl/fl}$ mice. $^{\#}$P ≤ 0.05, values significantly different from 5d-injured TA muscle of Ire1$^{fl/fl}$ mice. U, uninjured; I, injured.

FIGURE 3. Myofiber-specific ablation of IRE1α reduces abundance of satellite cells in injured muscle. (**A**) Representative photomicrographs of uninjured and 5d-injured TA muscle sections of Ire1$^{fl/fl}$ and Ire1^{mKO} mice after immunostaining for Pax7 (red) and laminin (green) protein. Nuclei were identified by staining with DAPI. Scale bar: 50 µm. White arrows point to Pax7^{+} satellite cells. (**B**) Average number of Pax7^{+} cells per field (~0.15 mm^{2}) in uninjured and 5d-injured TA muscle of Ire1$^{fl/fl}$ and Ire1^{mKO} mice. (**C**) Relative mRNA levels of Pax7 in uninjured and 5d-injured TA muscle of Ire1$^{fl/fl}$ and Ire1^{mKO} mice assayed by performing qPCR (n=3 for Uninjured Ire1$^{fl/fl}$, n=3 for Uninjured Ire1^{mKO}, n=4 for Injured Ire1$^{fl/fl}$ and n=5 for Injured Ire1^{mKO} group). (**D**) Representative immunoblots showing levels of Pax7 and unrelated protein GAPDH in uninjured and 5d-injured TA muscle of Ire1$^{fl/fl}$ and Ire1^{mKO} mice. (**E**) Primary mononuclear cells were isolated from TA muscle of Ire1$^{fl/fl}$ and Ire1^{mKO} mice and subjected to FACS analysis for satellite cells. Representative FACS dot plots demonstrating the percentage of α7-integrin^{+} cells in 5d-injured TA muscle of Ire1$^{fl/fl}$ and Ire1^{mKO} mice. (**F**) Quantification of α7-integrin^{+} satellite cells in uninjured and 5d-injured TA muscle of Ire1$^{fl/fl}$ and Ire1^{mKO} mice assayed by FACS (n=4 in each group). Data are expressed as mean ± SEM and analyzed by one-way analysis of variance (ANOVA) followed by Tukey's multiple comparison test. *****P≤0.05, values significantly different from uninjured TA muscle of Ire1$^{fl/fl}$ mice. $^{\#}$P ≤ 0.05, values significantly different from 5d-injured TA muscle of Ire1$^{fl/fl}$ mice. U, uninjured; I, injured.

FIGURE 4. IRE1α promotes proliferation of satellite cells. (**A**) Left side TA muscle of Ire1$^{fl/fl}$ and Ire1^{mKO} mice was given intramuscular injection of 1.2% $BaCl_2$ solution. After 3 days, the

mice were given an intraperitoneal injection of EdU and 11 days later, the TA muscles were collected and muscle sections prepared were stained to detect EdU, laminin, and nuclei. Representative photomicrographs of TA muscle sections after EdU, anti-laminin, and DAPI staining are presented here. Scale bar: 50 µm. (**B**) Average number of EdU^+ nuclei per myofiber and (**C**) percentage of myofibers containing 2 or more centrally located EdU^+ nuclei in TA muscle of $Ire1^{fl/fl}$ and $Ire1^{mKO}$ mice (n=4 mice per group). Data are presented as mean ± SEM. *****P≤0.05, values significantly different from corresponding TA muscle of $Ire1^{fl/fl}$ mice by unpaired t test. (**D**) Single myofibers were isolated from the EDL muscle of $Ire1^{fl/fl}$ and $Ire1^{mKO}$ mice and cultured for 72 h. Representative images of myofiber-associated cells after immunostaining for Pax7 (red) and MyoD (green) protein. Nuclei were counterstained with DAPI (blue). Scale bar: 20 µm. Average number of (**E**) cellular clusters per myofiber, (**F**) cells per cluster, (**G**) $Pax7^{+/}MyoD^-$ cells per cluster, (**H**) $Pax7^{-/}MyoD^+$ cells per cluster, and (**I**) $Pax7^+/MyoD^+$ cells per cluster in $Ire1^{fl/fl}$ and $Ire1^{mKO}$ cultures. (**J**) In a separate experiment, single myofibers after being cultured for 72 h were pulse labelled with EdU for 90 min and then immunostained for Pax7 protein and detection of EdU incorporation. Average number of $Pax7^+/EdU^+$ cells per cluster on $Ire1^{fl/fl}$ and $Ire1^{mKO}$ myofibers (n=3 mice per group). Data are presented as mean ± SEM. *****P≤0.05, values significantly different from myofiber cultures prepared from $Ire1^{fl/fl}$ mice.

FIGURE 5. Myofiber-specific ablation of XBP1 in mice inhibits skeletal muscle regeneration. Left side TA muscle of $Xbp1^{fl/fl}$ and $Xbp1^{mKO}$ mice was injured by intramuscular injection of 50 µl of 1.2% $BaCl_2$ solution whereas right side TA muscle was injected with saline and served as control. The muscles were harvested at day 5 and 14 post-$BaCl_2$ injection. (**A**) Representative photomicrographs of H&E-stained sections of 5d- and 14d-injured TA muscle of $Xbp1^{fl/fl}$ and $Xbp1^{mKO}$ mice. Scale bar: 20 µm. Quantification showing (**B**) Average myofiber CSA (n=6 mice per group) (**C**) average Minimal Feret's diameter (n=6 mice per group), and (**D**) Percentage of myofibers containing 2 or more centrally located nuclei in TA muscle of $Xbp1^{fl/fl}$ and $Xbp1^{mKO}$ mice at day 5 post-injury. Quantification of average (**E**) myofiber CSA and (**F**) minimal Feret's diameter in TA muscle of $Xbp1^{fl/fl}$ and $Xbp1^{mKO}$ mice at day 14 post-injury. (n=5 for Injured $Xbp1^{fl/fl}$ and n=4 for Injured $Xbp1^{mKO}$ group) (**G**) Representative photomicrographs of 5d-injured TA muscle sections from $Xbp1^{fl/fl}$ and $Xbp1^{mKO}$ mice after

immunostaining for Pax7 (red) and laminin (green) protein. Nuclei were stained with DAPI (blue). Scale bar: 20 µm. (**H**) Average number of $Pax7^+$ cells per field (~0.15 mm^2) in 5d-injured TA muscle of $Xbp1^{fl/fl}$ and $Xbp1^{mKO}$ mice n=4 mice per group. Data are presented as mean ± SEM. *****P≤0.05, values significantly different from myofiber cultures prepared from $Ire1^{fl/fl}$ mice. (**I**) Relative levels of Pax7 mRNA in uninjured and 5d-injured TA muscle of $Xbp1^{fl/fl}$ and $Xbp1^{mKO}$ mice. Data are presented as mean ± SEM and analyzed by one-way analysis of variance (ANOVA) followed by Tukey's multiple comparison test. *****P≤0.05, values significantly different from uninjured TA muscle of $Xbp1^{fl/fl}$ mice. $^{\#}P \leq 0.05$, values significantly different from 5d-injured TA muscle of $Xbp1^{fl/fl}$ mice.

FIGURE 6. IRE1α regulates Notch signaling during skeletal muscle regeneration. TA muscle of $Ire1^{fl/fl}$ and $Ire1^{mKO}$ mice were injected with 1.2% $BaCl_2$ solution. After 5d, the muscles were isolated and processed for qPCR and western blot analysis. Relative mRNA levels of (**A**) Notch receptors Notch1, Notch2, and Notch3; (**B**) Notch ligands Jagged1, Jagged2, DLL1, and DLL2; and (**C**) Notch targets Hes1, Hes6, Hey1 and HeyL in 5d-injured TA muscle of $Ire1^{fl/fl}$ and $Ire1^{mKO}$ mice (n=8-9 per group). (**D**) Immunoblot presented here demonstrate protein levels of Notch1, Hes6, and unrelated protein GAPDH in uninjured and 5d-injured TA muscle of $Ire1^{fl/fl}$ and $Ire1^{mKO}$ mice. Relative mRNA levels of (**E**) Wnt ligands Wnt4, Wnt5A, Wnt7A and Wnt11; (**F**) Wnt receptors Fzd1, Fzd2, Fzd4, and Fzd6, and (**G**) Wnt targets Axin2 in 5d-injured TA muscle of $Ire1^{fl/fl}$ and $Ire1^{mKO}$ mice (n=5 per group). Data are presented as mean ± SEM. *****P≤0.05, values significantly different from corresponding 5d-injured TA muscle of $Ire1^{fl/fl}$ mice.

FIGURE 7. IRE1α regulates NF-κB signaling in regenerating myofibers. Left side TA muscle of $Ire1^{fl/fl}$ and $Ire1^{mKO}$ mice was given intramuscular injection of 1.2% $BaCl_2$ solution whereas right side TA muscle was injected with saline alone. After 5 days, the TA muscles were harvested and processed by western blotting and qPCR. (**A**) Representative immunoblots presented her demonstrate the levels of p-p65, p65, p100, p52 and unrelated protein GAPDH in uninjured and 5d-injured TA muscle of $Ire1^{fl/fl}$ and $Ire1^{mKO}$ mice. Quantification of levels of (**B**) p-p65 and p65 (**C**) p100 and p52 protein (n=3 or 4 mice per group). Data are presented as mean ± SEM and analyzed by one-way analysis of variance (ANOVA) followed by Tukey's multiple

comparison test. *****P≤0.05, values significantly different from uninjured TA muscle of Ire1$^{fl/fl}$ mice. $^{\#}$P ≤ 0.05, values significantly different from 5d-injured TA muscle of Ire1$^{fl/fl}$ mice. (**D**) Relative mRNA levels of TNF-α, TNFR1, TNFR2, TWEAK, Fn14, IL-4, IL-6, and IL-10 in 5d-injured TA muscle of Ire1$^{fl/fl}$ and Ire1^{mKO} mice (n=6 mice per group). Data are presented as mean ± SEM. *****P≤0.05, values significantly different from 5d-injured TA muscle of Ire1$^{fl/fl}$ mice. U, uninjured; I, injured.

FIGURE 8. Myofiber-specific ablation of IRE1α exacerbates myopathy in mdx mice. (**A**) Western blots showing the levels of p-IRE1, IRE1, sXBP1 and unrelated protein GAPDH in TA muscle of 12-week old wild-type (WT) and mdx mice. (**B**) Densitometry analysis showing levels of p-IRE1, IRE1, sXBP1 and GAPDH protein in TA muscle of wild-type and mdx mice (n=3 in each group). *P<0.05, values significantly different from WT mice. (**C**) Average body weight, and (**D**) Four limb grip strength normalized with body weight of 10-week old mdx;Ire1$^{fl/fl}$ and mdx;Ire1^{mKO} mice (n=3 in each group). (**E**) Representative photomicrographs of H&E-stained TA muscle section from 10-week old mdx;Ire1$^{fl/fl}$ and mdx;Ire1^{mKO} mice. Scale bar: 50 µm. (**F**) Average myofiber CSA and (**G**) percentage of myofibers containing ≥2 nuclei in TA muscle of mdx;Ire1$^{fl/fl}$ and mdx;Ire1^{mKO} mice (n=4 in each group). (**H**) Representative photomicrographs of TA muscle sections after immunostaining for Pax7 (red) and laminin (green) protein. Nuclei were stained with DAPI (blue). Scale bar: 50 µm. White arrows point to Pax7^{+} satellite cells. (**I**) Frequency of Pax7^{+} cells per centrally nucleated myofibers in TA muscle of mdx;Ire1$^{fl/fl}$ and mdx;Ire1^{mKO} mice (n=4 in each group). (**J**) Relative mRNA levels of Pax7 in TA muscle of mdx;Ire1$^{fl/fl}$ and mdx;Ire1^{mKO} mice assayed by performing qPCR (n=5 in each group). Data are presented as mean ± SEM. *****P≤0.05, values significantly different from TA muscle of mdx;Ire1$^{fl/fl}$ mice.

FIGURE 1

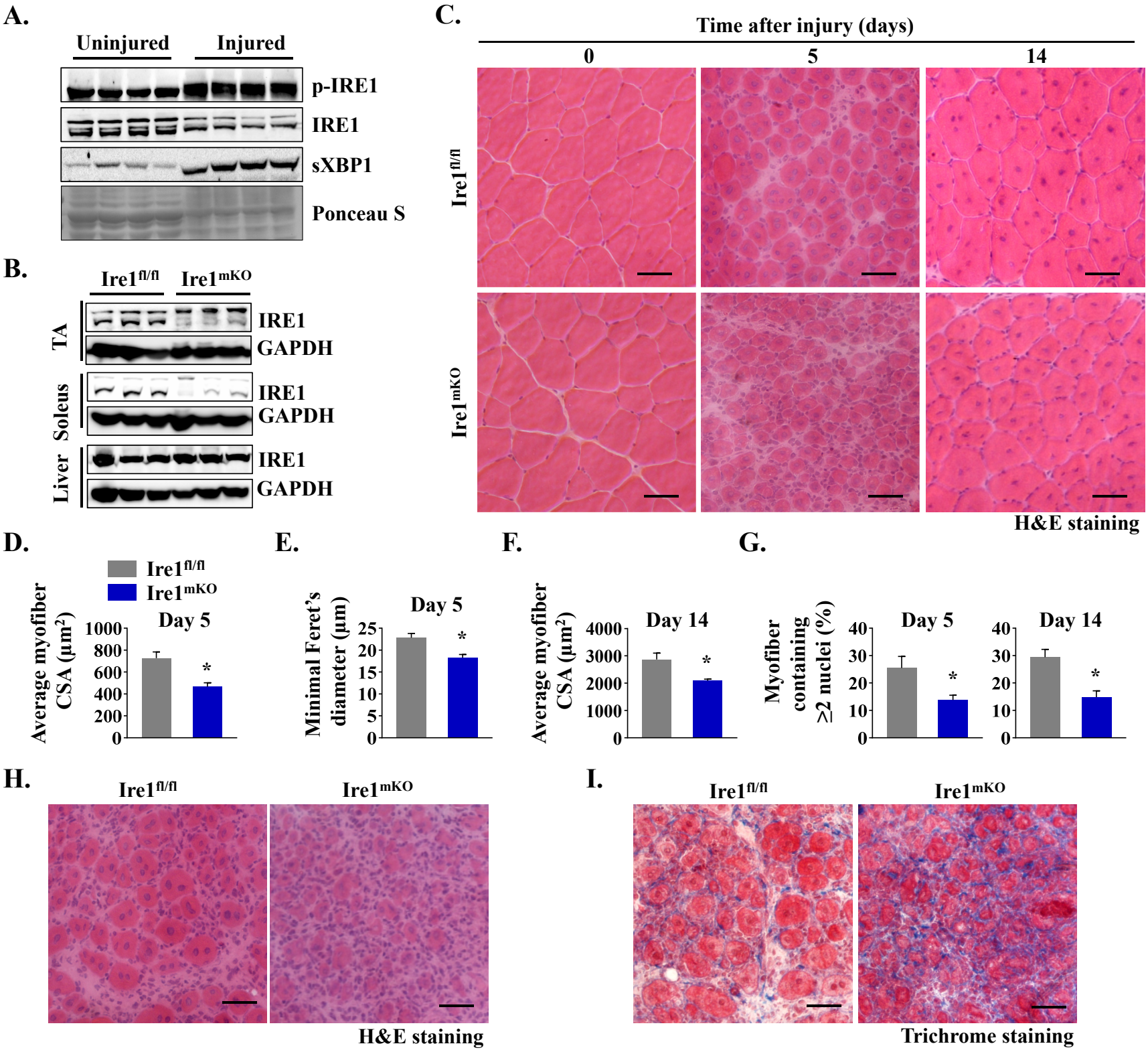
A.
Uninjured
Injured
p-IRE1
IRE1
sXBP1
Ponceau S
B.
Ire1fl/fl
Ire1mKO
TA
IRE1
GAPDH
Soleus
IRE1
GAPDH
Liver
IRE1
GAPDH
C.
Time after injury (days)
0
5
14
Ire1fl/fl
Ire1mKO
H&E staining
D.
Ire1fl/fl
Ire1mKO
Day 5
Average myofiber CSA (μm2)
1000
800
600
400
200
0
*
E.
Day 5
Minimal Feret's diameter (μm)
25
20
15
10
5
0
*
F.
Day 14
Average myofiber CSA (μm2)
4000
3000
2000
1000
0
*
G.
Day 5
Day 14
Myofiber containing ≥2 nuclei (%)
40
30
20
10
0
*
H.
Ire1fl/fl
Ire1mKO
H&E staining
I.
Ire1fl/fl
Ire1mKO
Trichrome staining

FIGURE 2

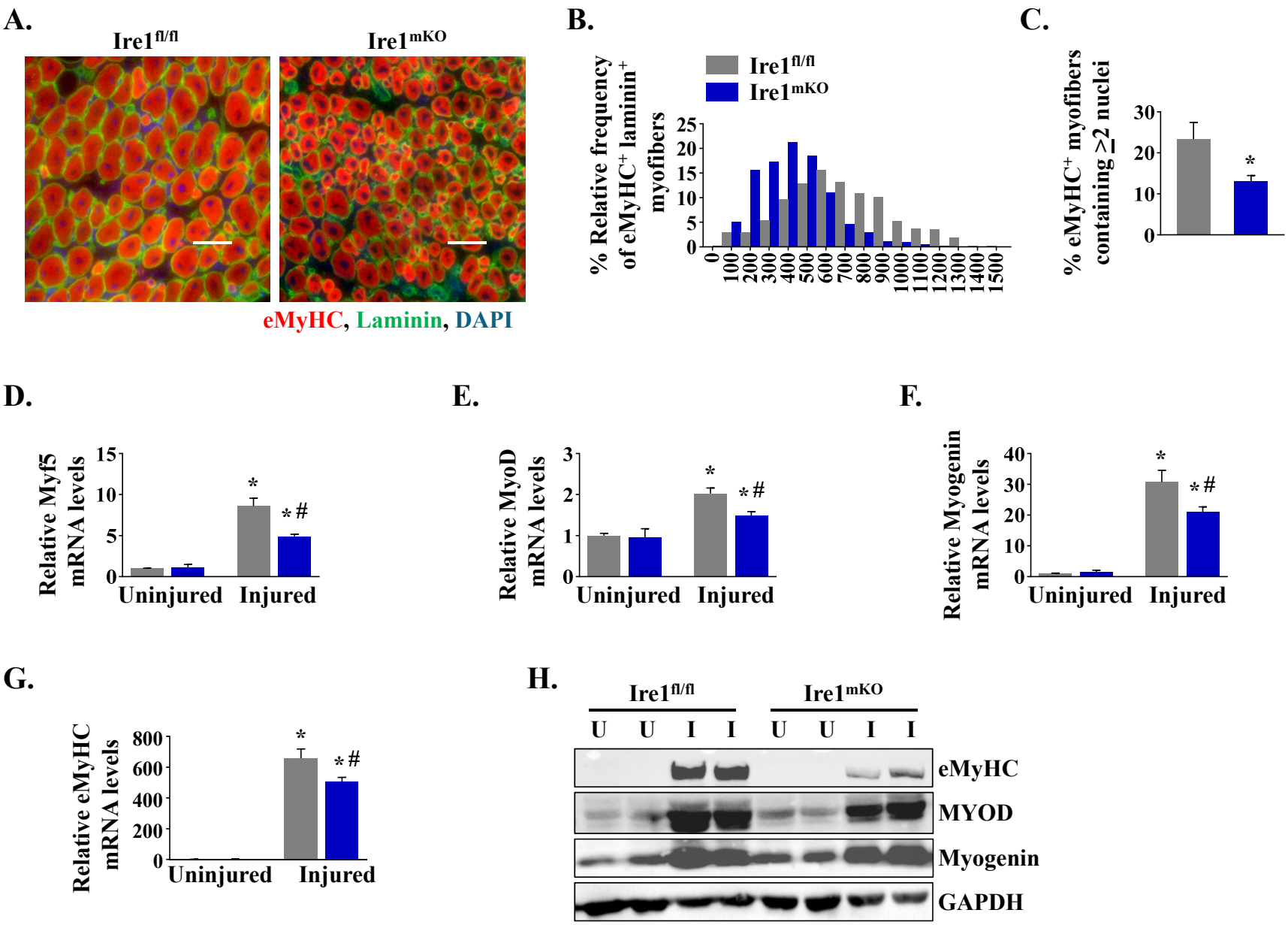
A.
Ire1fl/fl
Ire1mKO
eMyHC, Laminin, DAPI
B.
Ire1fl/fl
Ire1mKO
% Relative frequency of eMyHC+ laminin+ myofibers
0 100 200 300 400 500 600 700 800 900 1000 1100 1200 1300 1400 1500
C.
% eMyHC+ myofibers containing ≥2 nuclei
D.
Relative Myf5 mRNA levels
Uninjured
Injured
E.
Relative MyoD mRNA levels
Uninjured
Injured
F.
Relative Myogenin mRNA levels
Uninjured
Injured
G.
Relative eMyHC mRNA levels
Uninjured
Injured
H.
Ire1fl/fl
Ire1mKO
U U I I U U I I
eMyHC
MYOD
Myogenin
GAPDH

FIGURE 3

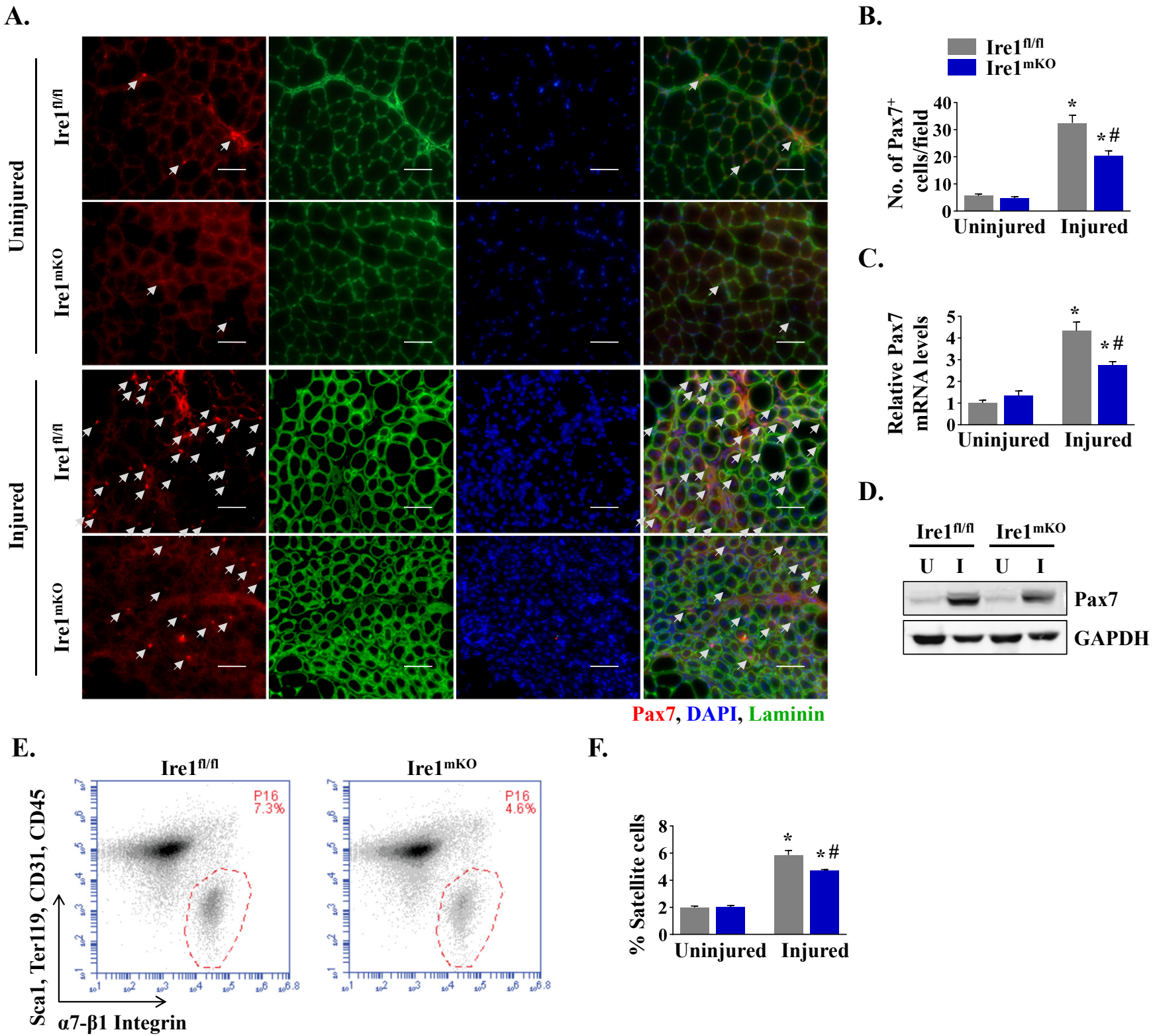
A.
Uninjured
Injured
Ire1fl/fl
Ire1mKO
Pax7, DAPI, Laminin
B.
Ire1fl/fl
Ire1mKO
No. of Pax7+ cells/field
Uninjured
Injured
C.
Relative Pax7 mRNA levels
Uninjured
Injured
D.
Ire1fl/fl
Ire1mKO
U I U I
Pax7
GAPDH
E.
Ire1fl/fl
Ire1mKO
P16 7.3%
P16 4.6%
Sca1, Ter119, CD31, CD45
α7-β1 Integrin
F.
% Satellite cells
Uninjured
Injured

FIGURE 4

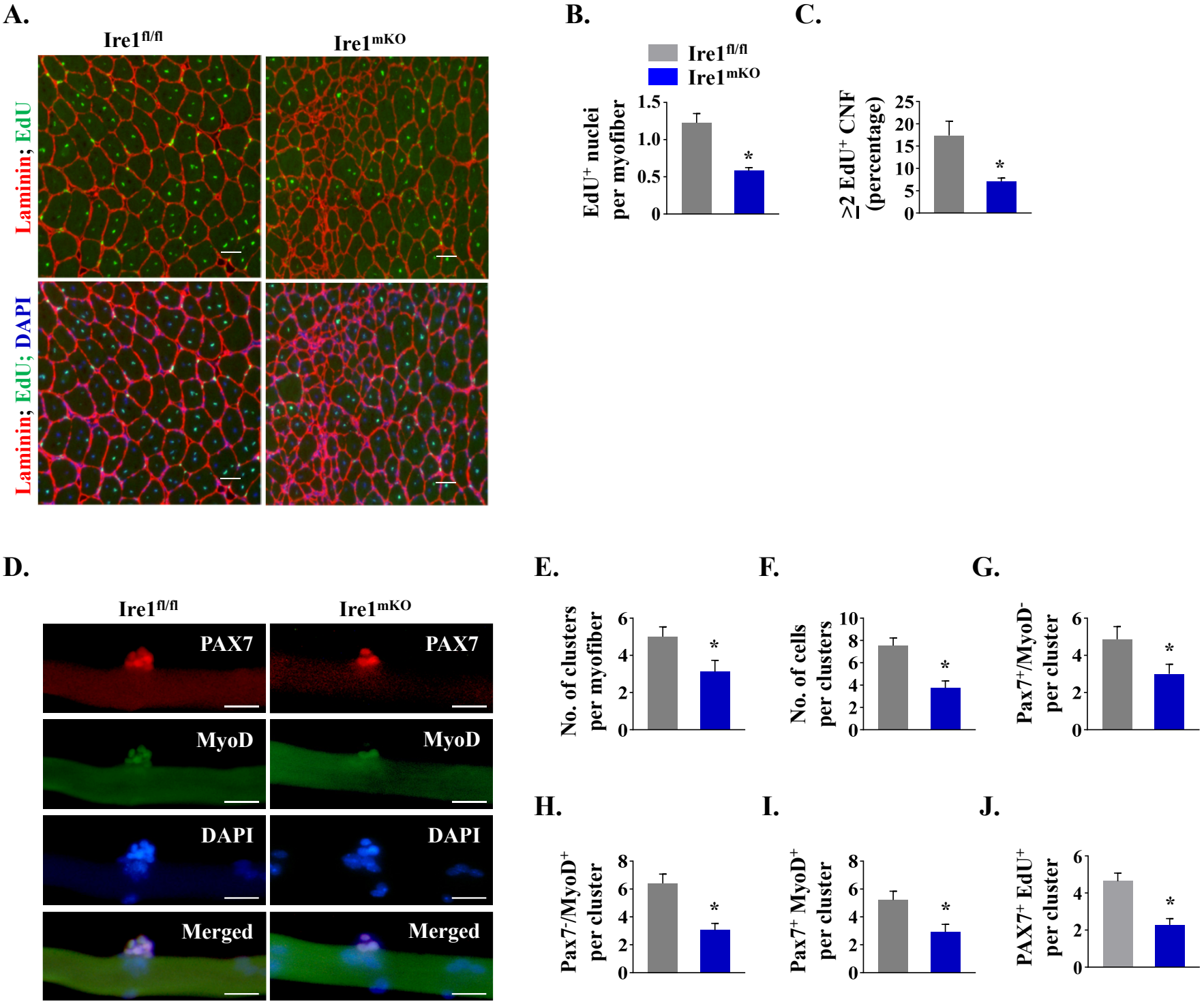
A.
Ire1fl/fl
Ire1mKO
Laminin; EdU
Laminin; EdU; DAPI
B.
Ire1fl/fl
Ire1mKO
EdU+ nuclei per myofiber
1.5
1.0
0.5
0
*
C.
≥2 EdU+ CNF (percentage)
25
20
15
10
5
0
*
D.
Ire1fl/fl
Ire1mKO
PAX7
MyoD
DAPI
Merged
E.
No. of clusters per myofiber
6
4
2
0
*
F.
No. of cells per clusters
10
8
6
4
2
0
*
G.
Pax7+/MyoD- per cluster
6
4
2
0
*
H.
Pax7-/MyoD+ per cluster
8
6
4
2
0
*
I.
Pax7+ MyoD+ per cluster
8
6
4
2
0
*
J.
PAX7+ EdU+ per cluster
6
4
2
0
*

FIGURE 5

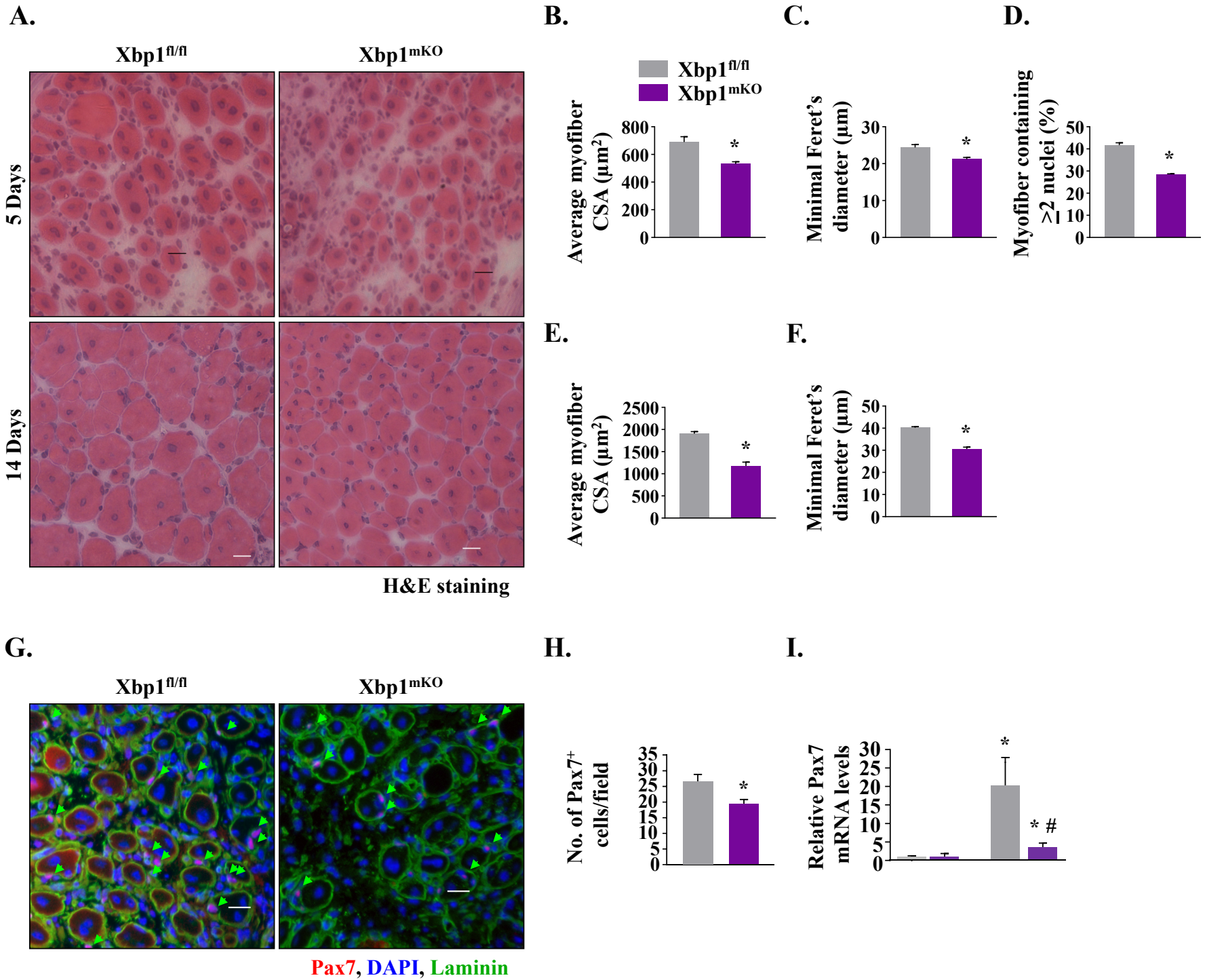
A.
Xbp1fl/fl
Xbp1mKO
5 Days
14 Days
H&E staining
B.
Xbp1fl/fl
Xbp1mKO
Average myofiber CSA (µm2)
800
600
400
200
0
*
C.
Minimal Feret's diameter (µm)
30
20
10
0
*
D.
Myofiber containing ≥2 nuclei (%)
50
40
30
20
10
0
*
E.
Average myofiber CSA (µm2)
2500
2000
1500
1000
500
0
*
F.
Minimal Feret's diameter (µm)
50
40
30
20
10
0
*
G.
Xbp1fl/fl
Xbp1mKO
Pax7, DAPI, Laminin
H.
No. of Pax7+ cells/field
35
30
25
20
15
10
5
0
*
I.
Relative Pax7 mRNA levels
30
25
20
15
10
5
0
*
* #

FIGURE 6

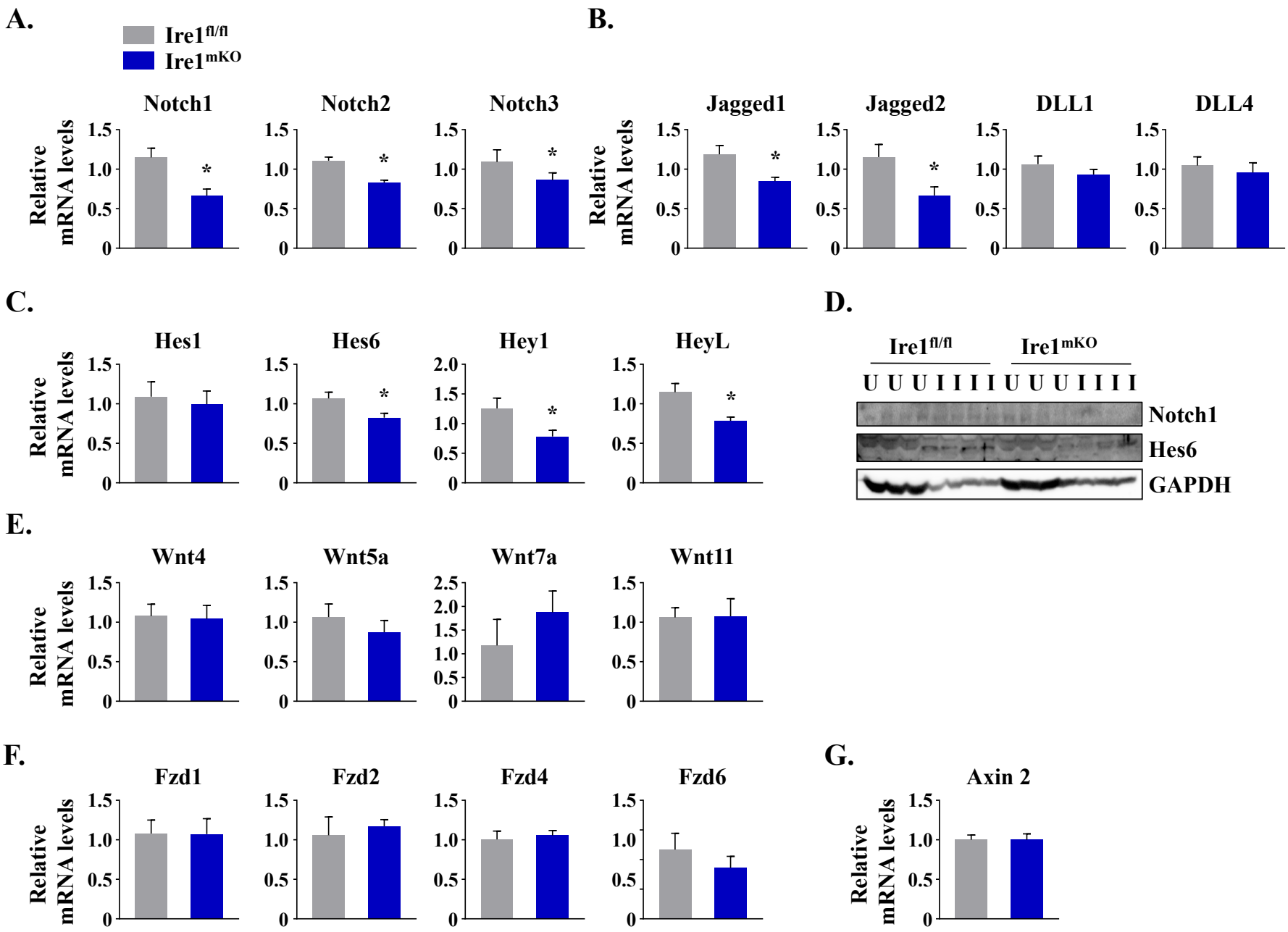
A.
Ire1fl/fl
Ire1mKO
Notch1
Notch2
Notch3
Relative mRNA levels
B.
Jagged1
Jagged2
DLL1
DLL4
C.
Hes1
Hes6
Hey1
HeyL
D.
Ire1fl/fl
Ire1mKO
U U U I I I I U U U I I I I
Notch1
Hes6
GAPDH
E.
Wnt4
Wnt5a
Wnt7a
Wnt11
F.
Fzd1
Fzd2
Fzd4
Fzd6
G.
Axin 2

FIGURE 7

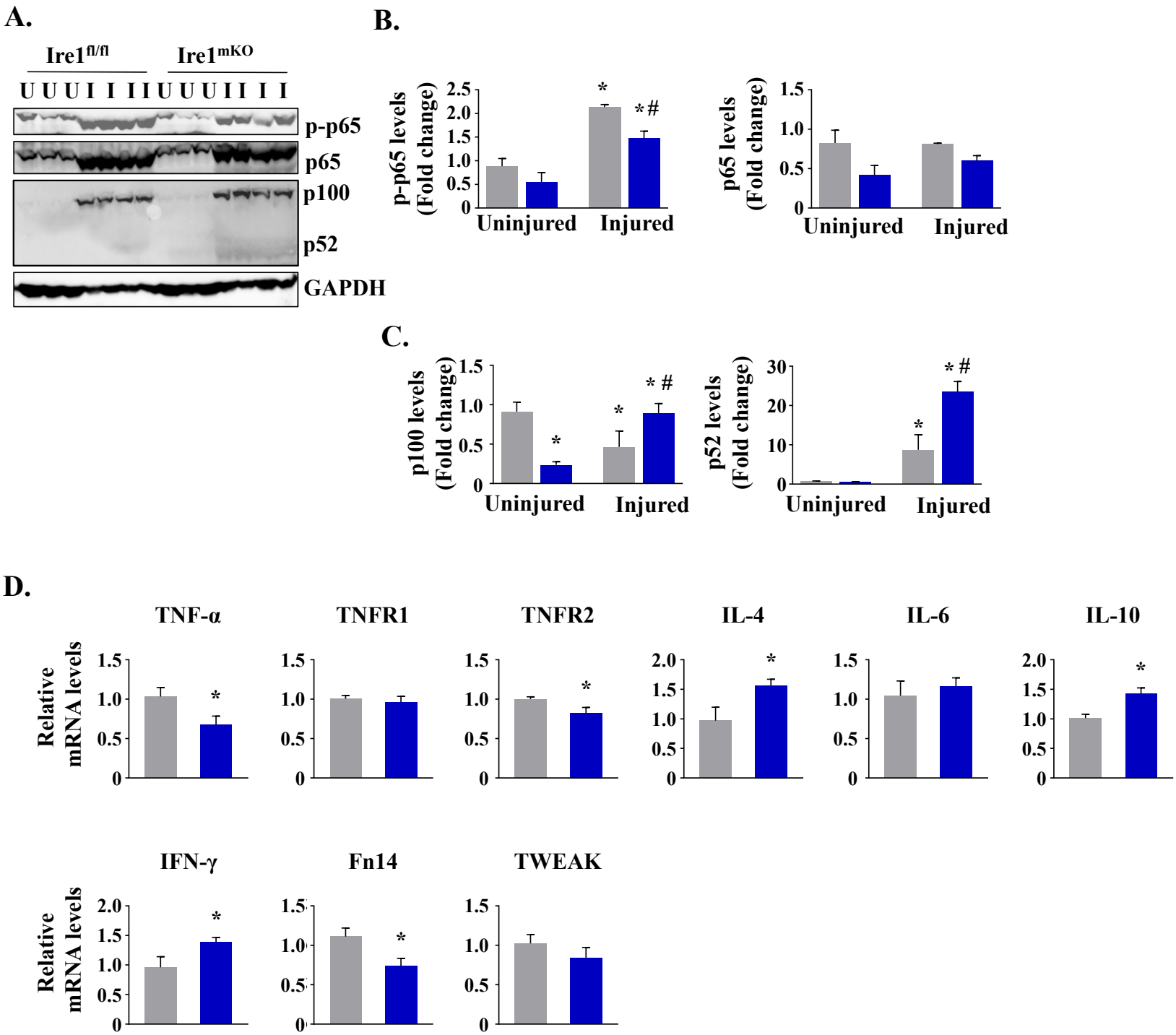
A.
Ire1fl/fl
Ire1mKO
U U U I I I I U U U I I I I
p-p65
p65
p100
p52
GAPDH
B.
p-p65 levels (Fold change)
Uninjured
Injured
p65 levels (Fold change)
C.
p100 levels (Fold change)
p52 levels (Fold change)
D.
TNF-α
TNFR1
TNFR2
IL-4
IL-6
IL-10
IFN-γ
Fn14
TWEAK
Relative mRNA levels

FIGURE 8

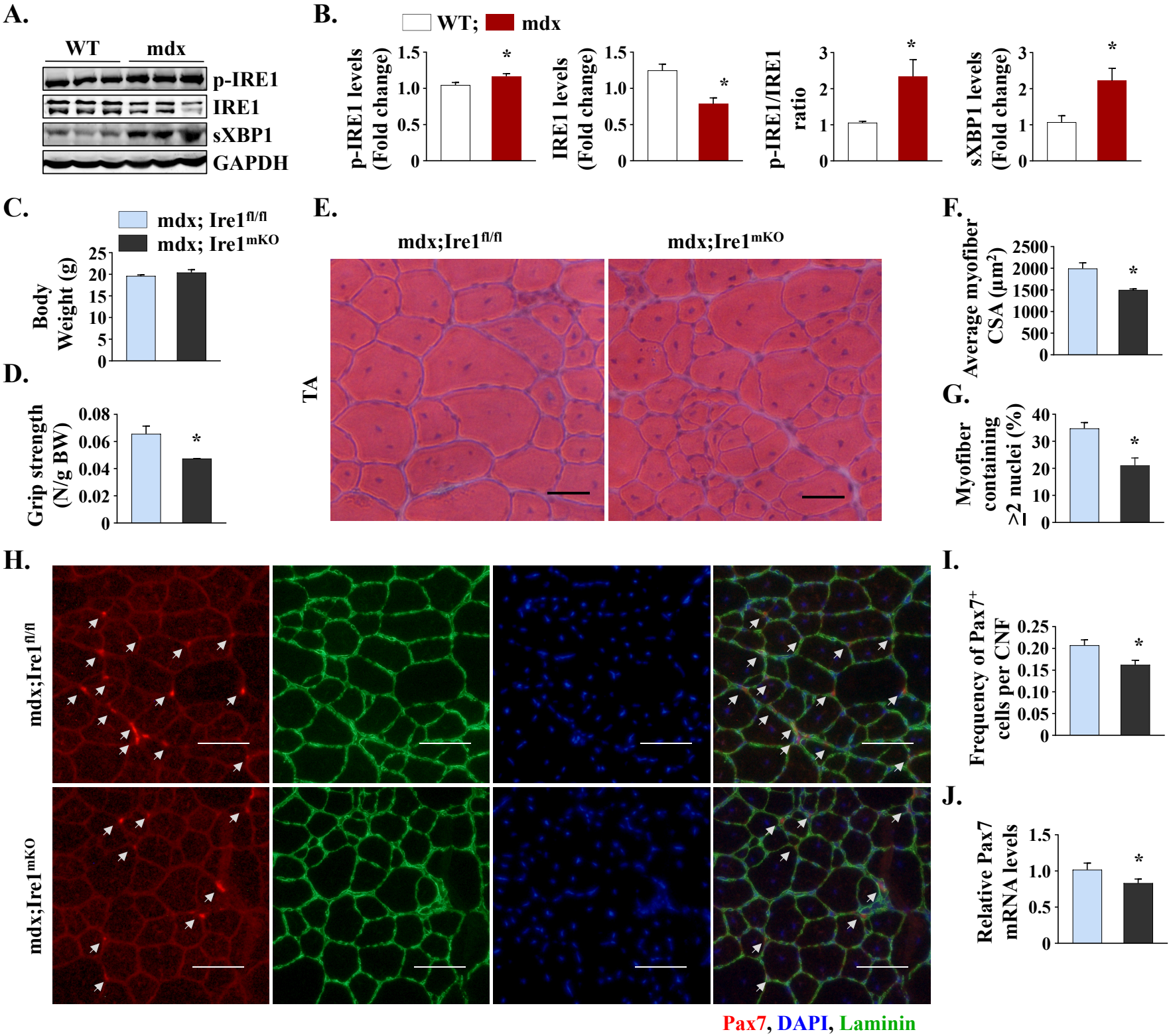
A.
WT
mdx
p-IRE1
IRE1
sXBP1
GAPDH
B.
WT; mdx
p-IRE1 levels (Fold change)
IRE1 levels (Fold change)
p-IRE1/IRE1 ratio
sXBP1 levels (Fold change)
C.
mdx; Ire1fl/fl
mdx; Ire1mKO
Body Weight (g)
D.
Grip strength (N/g BW)
E.
mdx;Ire1fl/fl
mdx;Ire1mKO
TA
F.
Average myofiber CSA (μm2)
G.
Myofiber containing ≥1 nuclei (%)
H.
mdx;Ire1fl/fl
mdx;Ire1mKO
Pax7, DAPI, Laminin
I.
Frequency of Pax7+ cells per CNF
J.
Relative Pax7 mRNA levels